Miguel Duarte Dias Francisco

Shaping Animal Design

The role of Hoxd13 targets in the evolution of Vertebrate limbs

Universidade do Algarve

Faculdade de Ciências e Tecnologias

2021

Miguel Duarte Dias Francisco

Shaping Animal Design

The role of Hoxd13 targets in the evolution of Vertebrate limbs

Mestrado em Biologia Molecular e Microbiana

Trabalho efetuado sob a orientação de:

Prof.ª Dr.ª Renata Freitas, Universidade do Porto

Prof.ª Dr.ª Raquel Andrade, Universidade do Algarve

Universidade do Algarve

Faculdade de Ciências e Tecnologias

2021

Shaping Animal Design

The role of Hoxd13 targets in the evolution of Vertebrate limbs

Declaração de Autoria do Trabalho

Declaro ser o autor deste trabalho, que é original e inédito. Autores e trabalhos consultados estão devidamente citados no texto e constam da listagem de referências incluída.

Miguel Duarte Dias Francisco

.....

(assinatura)

Dedicatória e Agradecimentos

O meu muito sincero obrigado às minhas orientadoras Prof.ª Dr.ª Renata Freitas e Prof.ª Dr.ª Raquel Andrade pela disponibilidade sempre demonstrada e pela perícia e responsabilidade com que me orientaram neste projeto de dissertação de mestrado. Um grande agradecimento aos meus colegas de laboratório e amigos, Francisco Cadete, Joana Castro e Raquel Ramos pela ajuda prestada, tanto no laboratório como fora do mesmo.

Um agradecimento muito sentido aos meus pais e família por me terem acompanhado ao longo, não só desta tese, mas de todo o percurso que me trouxe até aqui. Sempre me apoiaram e deram força para continuar no meu caminho, mesmo quando a saudade dos que estão longe da vista, mas sempre no coração, aperta.

Obrigado à minha namorada Inês Meirinho por ter embarcado comigo nesta aventura e me ter sempre apoiado incondicionalmente ao longo da mesma.

Uma última gratidão para com o meu grande amigo Bruno Neto que, apesar de longe, também sempre demonstrou o seu completo apoio e ombro amigo.

A todos, o meu muito obrigado.

Resumo

Durante este projeto, explorámos novas hipóteses nas áreas de Biologia do Desenvolvimento e Evolução, numa tentativa de explicar a transição anatómica que ocorreu entre as barbatanas dos peixes e os membros dos tetrápodes. Este processo envolveu uma redução da área dérmica das barbatanas ("finfold"), bem como uma expansão das estruturas ósseas distais. Assim, a nossa hipótese propõe que genes envolvidos na rede *Hoxd13*, que são conhecidos por estar envolvidos no processo de formação dos membros, sofreram um processo de aumento de expressão durante a evolução, o que levou a que novas estruturas ósseas fossem progressivamente desenvolvidas na parte distal da barbatana/membro tetrápode.

Com este fim, estudámos três linhagens diferentes de peixe-zebra: 1) linha selvagem (*wtAB*); 2) linha transgénica que sobre expressa *hoxd13a* (*hoxd13* +++) e apresenta "finfolds" mais curtas; e 3) linha mutante que tem uma extensão das "finfolds" (Leo^{t1}/Lof^{dt2}). Esta segunda linha possui uma mutação em certos canais de potássio, o que altera o potencial de membrana das células. Esta simples alteração pode levar a uma descompensação de vários processos celulares e genéticos, sendo que não era conhecido que processo levaria a uma expansão da "finfold" nestes peixes.

Neste trabalho, analisámos alterações nos níveis de expressão de genes envolvidos na formação da barbatana/membro tetrápode durante o desenvolvimento embrionário por meio de técnicas de RT-qPCR e de hibridização *in situ*. O nosso principal objetivo foi estudar genes envolvidos na rede *Hoxd13*, analisando tanto alvos deste gene, como *bmp2b*, antagonistas dos seus alvos, tais como *smoc1, smoc2, noggin3* e *gremlin1a* e, por último, alvos da própria via de sinalização de BMP's, nomeadamente os genes *msx1b* e *msx2b*.

Primeiramente, verificámos que a linha mutante (Leo^{t1}/Lof^{dt2}) possui uma "finfold" evidentemente maior do que a condição selvagem durante o desenvolvimento, sendo que esta diferença já é bastante visível em estadios prematuros, a partir de 56 horas pós-fertilização (hpf), e torna-se cada vez mais acentuada com o decorrer do desenvolvimento. Utilizámos marcadores para o gene *actinodin1b* (*and1*) que codifica uma proteína não colagénica que faz parte dos raios dérmicos da barbatana. De seguida, analisámos os níveis de *bmp2b*, bem como os níveis de proliferação, através do gene *ciclinb1* (*ccnb1*), e de apoptose, usando o marcador *caspase3* (*casp3*), sendo que ambos os genes estão envolvidos nos processos que representam. Dados do nosso laboratório já demonstravam que a linha transgénica com "finfolds" mais curtas apresentava uma maior expressão de *hoxd13a, bmp2b* e *casp3*, bem como níveis inferiores de *ccnb1*, quando

comparados com a linha selvagem. Contribuímos na avaliação destes mesmos genes na linha mutante, sendo que esta apresenta "finfolds" maiores, relacionados com níveis mais baixos de *hoxd13a, bmp2b, casp3* e *ccnb1* em relação à condição selvagem. Estes resultados foram publicados em (Castro et al., 2021).

Decidimos também analisar outros genes envolvidos nesta rede para ver os seus níveis de expressão e a sua relação com o tamanho do "finfold". Os nossos resultados sugerem que existem flutuações relevantes dos genes acima mencionados, quer entre linhas estudadas, quer entre diferentes estadios dentro da mesma linha, incluindo a linha selvagem. Assim, contruímos a nossa hipótese de que a modulação das vias de sinalização de BMP's pode ter sido o mecanismo que levou a uma redução do "finfold" durante a evolução. Esta modulação também deve ter sido importante para controlar a apoptose na "apical ectordermal ridge" (AER) e na formação dos dígitos. Neste processo, estão envolvidos os genes *msx1b* e *msx2b*. Encontrámos uma relação entre maiores níveis de expressão de *msx2b*, o que sugere maior apoptose, e menor "finfold" nas barbatanas das linhas transgénicas e selvagem, enquanto a linha mutante apresenta menos expressão deste gene e maiores "finfolds". Sugerimos que este processo de controlo de apoptose estava presente no ancestral dos tetrápodes, que mais tarde o redirecionaram para a formação dos dígitos.

Outro resultado interessante foi que a sobre expressão de *hoxd13a* parece aumentar a expressão de vários intervenientes nesta rede, tais como *smad1, smoc1, noggin3* e *msx2b*. Nenhum destes genes está indicado como alvo de *hoxd13a* (Salsi et al., 2008), o que nos leva a querer que o impacto da expressão de *hoxd13a* nestes genes se dê de forma indireta. No entanto, já foi proposto que as proteínas Hoxd13 e Smad1 sejam cofatores em membros de ratinho (Williams et al., 2005). Isto pode sugerir que a modulação de apoptose, durante a evolução, pode ter sido devido a esta relação entre estas proteínas, que depois ativam genes de apoptose, como os genes *msx.*

Na linha Leo^{t1}/Lof^{dt2}, além das suas barbatanas peitorais mostrarem uma redução na expressão de *bmp2b*, encontrámos um aumento significativo na expressão de *smoc1* e *smoc2*. Visto que estes são antagonistas de genes *bmp*, sugerimos que os seus níveis de expressão altos são responsáveis pela redução da expressão de *bmp2b*, em conjunto com níveis baixos de *hoxd13a* (Castro et al., 2021). Os antagonistas *noggin3* e *gremlin1a* também apresentaram níveis maiores de expressão nesta linha, podendo contribuir para a redução de *bmp2b*.

Por fim, propomos que este pode não ser o único mecanismo envolvido no fenótipo de maior "finfold" da linha mutante. Ao comparar a expressão dos genes estudados entre estadios na mesma linha, formulámos uma hipótese alternativa; com exceção de *smad1*, todos os genes relacionados com as vias de sinalização de BMP's apresentam expressão muito baixa a 24hpf, seguidos de um pico de expressão a 48hpf. Na condição selvagem, este pico aparece mais cedo, às 24hpf. Isto sugere que a rede *hoxd13a/bmp* não é menos expressa nos mutantes, mas sim retardada no desenvolvimento. Isto pode também explicar o porquê de as barbatanas desta linha parecerem atrasadas no seu desenvolvimento e apresentarem uma morfologia que sugere uma manutenção no estado de proliferação de células na "finfold" durante mais tempo.

Os nossos resultados sugerem um novo mecanismo que pode ter levado à redução da área dérmica e expansão dos elementos ósseos distais nas barbatanas de peixes ancestrais, que, posteriormente, evoluíram para membros. Mostrámos que os genes envolvidos na rede *Hoxd13* mudam entre as linhas estudadas, mas também, e mais importante, entre os estadios de desenvolvimento. Obtivemos dados que mostram que a linha mutante é retardada no desenvolvimento, com a rede *Hoxd13* a iniciar apenas em estadios posteriores. Por outro lado, a condição transgénica é forçada a finalizar essa mesma rede mais cedo do que o suposto, devido ao tratamento de "heat shock". Isto pode levar a diferentes períodos de tempo em que as células proliferam em vez de se diferenciar, levando a uma "finfold" mais longa ou mais curta na barbatana. Pensamos que este fenómeno de deslocamento temporal pode ter sido o gatilho que levou ao desenvolvimento de estruturas ósseas distais progressivamente mais complexas nas barbatanas, culminando com o autopode característico dos tetrápodes.

Abstract

During this project, we explored new hypothesis in the fields of Developmental Biology and Evolution, aiming to explain the anatomical transition that occurred between fish fins and tetrapod limbs. This process involved a reduction in the dermal fold of the fins during development (finfold), and concomitant expansion of the distal bone structures. To this end, we used three different strains of zebrafish: 1) wild-type fish (*wtAB*); 2) transgenic fish that allow overexpression of *hoxd13a* (*hoxd13+++*) and, consequently, possess shorter finfolds; and 3) mutant fish which have longer finfolds (Leo^{t1}/Lof^{dt2}). We analyzed changes in gene expression levels that may be influenced by *hoxd13a* expression levels, particularly those associated with BMP signaling, during locomotory appendage formation, using RT-qPCR and *in situ* hybridization techniques. The results suggest a novel mechanism that may have led to the reduction of finfolds and expansion of distal bone elements in the tetrapod ancestor. We showed that genes associated with BMP signaling are expressed differently in the analyzed zebrafish strains, which are also characterized by distinct levels of *hoxd13a* expression. Furthermore, the expression dynamics of these genes throughout development were found to be distinct in these lines. We obtained data suggesting that the mutant line is developmentally delayed, having cells that may take longer to enter differentiation, and with *hoxd13a*-dependent molecular machinery being activated later, compared to wild-type. In contrast, the transgenic condition appears to have the *hoxd13a*-dependent molecular machinery strongly active after the induction of *hoxd13a* overexpression. These different timings can lead to distinct periods of cell proliferation followed by differentiation, which can influence the size of the finfolds. Thus, this phenomenon of time-shifting concerning the entry into the differentiation process may have been the trigger that led to shortening of finfolds and expansion of distal bone structures which later evolved to the autopod in tetrapods.

Keywords: Development, *Hoxd13*, Evolution, Fins, Tetrapod Limb.

TABLE OF CONTENTS

FIGURE INDEX

TABLE INDEX

LIST OF ABBREVIATIONS

BC	Before Christ
AD	Anno Domini
MYA	Million-years ago
LPM	Lateral Plate Mesoderm
PZ	Progress Zone
ZPA	Zone of Polarizing Activity
AER	Apical Ectodermal Ridge
RA	Retinoic Acid
Fgf	Fibroblast Growth Factor
Shh	Sonic hedgehog
Wnt	Wingless-related integration site
BMP	Bone Morphogenic Protein
Msx	Muscle Segment Homeobox
2WGD	2 Whole Genome Duplication Events
3WGD	3 Whole Genome Duplication Events
KO	Knockout
Hpf	Hours post-fertilization
Dpf	Days post-fertilization
wtAB	Wild-type AB line
ISH	*In situ* hybridization
PFA	Paraformaldehyde

PBT	Phosphate buffered saline with 0.01% Tween 20
PBS	Phosphate buffered saline
MeOH	Methanol
PCR	Polymerase Chain Reaction
TAE	Tris-acetate-EDTA buffer
RT	Room temperature
DIG	Digoxigenin
Hyb+	Hybridization mix containing yeast tRNA
Hyb-	Hybridization mix whitout yeast tRNA
SSC	Saline Sodium Citrate
BSA	Bovine Serum Albumin

1. INTRODUCTION

1.1 Developmental Biology, a science with history

According to embryology historians, the first observations that lead to the study of embryonic development occurred in the antiquity, in the Egyptian civilization, more than 1000 years before Christ (BC). The first written records of embryological studies are, however, attributed to the Greeks. Hippocrates (460BC–370BC) was the first to write about embryonic development, being the first to allude to the concept of "pre-formationism", instead of the idea that humans develop from perfect miniatures of the adult forms. However, it is Aristotle that is recognized as the truly first embryologist (384BC–322BC), due to his studies on different embryos from bird, mammalians, and "cold-blooded" embryos. Needham even suggests that Aristotle may have been the first to study human aborted embryos (Needham, 1959). He was also the first to suggest the idea of "recapitulation", observing that the young embryos of different species have common characteristics and that, as the embryos aged, distinguishable characteristics appeared.

After that, authors such as Galeon of Pergamos (129 Anno Domini (AD) to 216 AD) and Albert Magnus (1200-1280) gave contributions to embryology. However, an increasing tendency arose, replacing the scientific view by theology and speculative theories. This path was interrupted by Leonardo da Vinci (1452-1519), the first dissecting a human fetus and to perform quantitative measurements of embryos. Interestingly, in the early 1700, embryologists were divided into two groups: the ones that defended that organisms developed from eggs (ovists) and those who believed that small adult organisms existed in sperm (spermists). At that time, many advocated that human sperm cells carried inside a miniature of a human being, who would then grow inside the mother uterus, and they even claimed to have seen it under the microscope. This was the concept of "*Homunculus*" (Fig. 1.1), which means "little man" in Latin, and that was first proposed by Leeuwenhoek and Luiz Hamm, in 1667, based on their observations of sperm cells under the microscope. (Andrade-Rocha, 2017).

Nowadays, due to improvements in science and technology, we know that this theory cannot be plausible. It is now known that a new organism results from multiple divisions of a single cell, called zygote, and posterior differentiation of these cells in tissues, organs and systems, all of them composing a fully developed organism. However, this process is not so simple as it appears when we first look at it. In fact, the rise of a new being and the different complexity among all the

species is so intricate that a big part of it is still poorly understood, giving rise to new scientific questions (Kurosaka et al., 2017).

Due to the complexity of this research field, it is no longer possible to study it without dissecting it into smaller pieces, exploring various processes alone and then integrating them into the big and fascinating puzzle that allows explaining the formation of a *de novo* organism. Understanding the genetics involved in embryonic development can open new perspectives, such as studying embryopathies (Loucks & Ahlgren, 2012), congenital disorders, cancer (Garcia et al., 2020) and even evolution of animal morphology, answering questions such as how did the fin of a fish gave rise to the more complex and different tetrapod limb (Paço & Freitas, 2018).

Figure 1.1: “Homunculus” (draw by Hartsoeker, 1695).

1.2. Appendage evolution in Vertebrates

1.2.1 The first locomotory appendages in Vertebrates: unpaired finfolds

One of the physical characteristics more distinctive in the human being is our hands and fingers (autopods), and how we used them to "change the world". However, there is a very big and thrilling evolutionary history starting with the ancestors of Vertebrates found in the fossil record, such as the Invertebrate *Pikaia gracilens* (Fig. 1.2A). This early chordate appeared around 505 million-years ago (MYA), during the "Cambrian explosion" (Lacalli, 2012), and possessed a unique and continuous locomotory structure throughout the dorsal and ventral midlines, that resembled the finfold found in extant chordate lineages, such as the amphioxus (Fig. 1.2B). These ancient appendage-types have a simple morphology, allowing motility, but they seem to have evolved progressively to more complex and diverse structures, which could have new functions, such as swimming faster or turn direction more easily (Harris, 1936), walk on land, fly, catching things and grappling (Freitas et al., 2006).

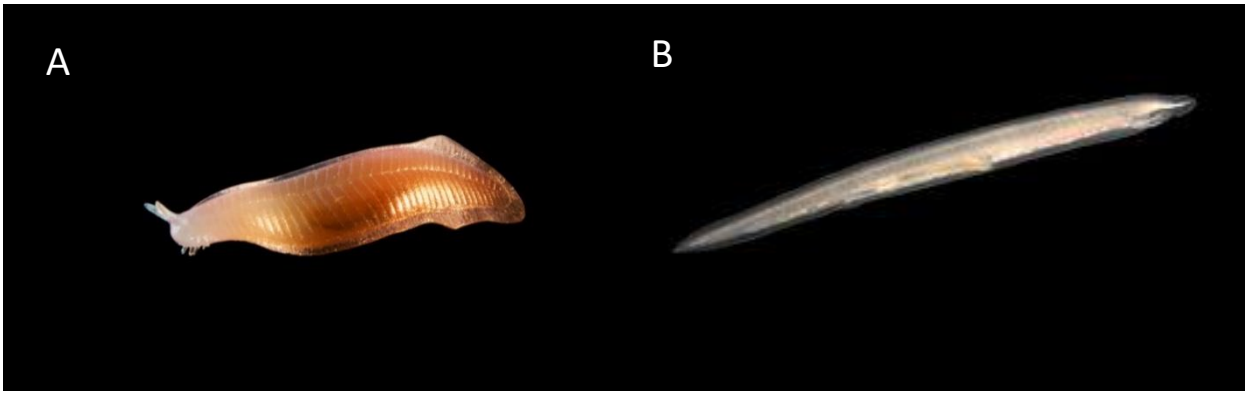

Figure 1.2 – *Pikaia gracilens* (A) and *Branchiostoma lanceolatum* representing amphioxus (B) reconstruction (http://www.10tons.dk).

To understand this process, we need to go back to the first fins of pre-historic fish. Some researchers defend the idea that, initially, fish had no individual paired and unpaired fins, but only a unique finfold that went all the way from the head to the tail end, dorsal and ventrally, and that resembles the finfold from chordates such as the amphioxus (Freitas et al., 2006). This finfold was mostly able to pull the fish forward, but if one could turn direction instead of just moving forward,

that one could move around better to catch prey or run from predators, giving it an evolutionary advantage. As so, selective pressure during evolution allowed the survival of fish that had more mobility, and the unique finfold gave rise, throughout time, to smaller individualized unpaired fins, dorsal and ventrally, and, probably later, paired fins and limbs, which grown from the lateral plate mesoderm (LPM). These novel appendages had new functions, allowing the fish to turn around (pectoral fins), to propel forward (caudal) or even help in mating (e.g. pelvic fins in sharks) (Freitas et al., 2014).

1.2.2 The origin of paired appendages

To start forming the limb bud, a mass of cells needs to migrate from the LPM, giving rise to 4 distinct buds, 2 pectoral and 2 pelvic (Zuniga, 2015). Two influential theories have been proposed in the past to explain how paired appendages evolved in Vertebrates.

The first one is the "fin-fold theory", defended in the 19th century by Thatcher (1877) and Balfour (1878) (Fig. 1.4B). It states that paired appendages evolved by subdivision of a finfold that also gave rise to unpaired appendages. This means that the ancestor of fish with paired appendages must have had 2 lateral fins running along the body. The fossil record shows that this happened, with the fish family of anaspids. The first anaspids, such as Pharyngolepis (Fig. 1.3A), had a long ventrolateral finfold, while later forms of this family, such as Rhyncholepis (Fig. 1.3B), possessed a shorter pair of fins in the pectoral region (Janvier, 1996).

Some studies in elephant sharks (Riley et al., 2017) and goldfish (Abe & Ota, 2017) have helped to sustain this theory. More recent theories have been proposed, based on this classical idea, that stat that paired appendages emerged from a field of competence inherited by the LPM during its evolution from a tissue that was already competent to form unpaired fins: the dorsal and ventral paraxial mesoderm (Freitas et al., 2006, 2014).

The second theory is known as the "gill arch theory" (Fig. 1.4A) and explains that pectoral appendages arose from modifications of the gill arches more distal to the jaw, and then pelvic appendages "copied" the morphological network program during evolution. It has its foundations in the comparative anatomy of the gill arches and pectoral fins in some fish species. Due to the anatomical and genetic similarity observed between the pectoral and pelvic fins, the second ones

could have resulted from a duplication of the developmental mechanisms present in the pectoral fins, but re-iterated at a posterior location (Diogo, 2020). Due to the lack of proof, this theory was set aside until recently, when a conserved molecular mechanism between the formation of the gill arch and pectoral fins was discovered, suggesting a common developmental origin for these two structures (Nagashima et al., 2016).

The fossil record suggests that paired fish fins suffered sequential changes in the distal endoskeleton that culminated with the development of limbs, multi-fingered structures that appeared in stem-tetrapods (Fig. 1.5) (Freitas et al., 2014; Woltering et al., 2020). This evolutionary process designated as the *fin-to-limb* transition probably had an enormous impact on the colonization of the land by Vertebrates in the Devonian period, around 380 MYA. The fossil that better represents the transition between these two anatomical structures is the sarcopterygian *Tiktaalik roseae*, (Fig. 1.6) found in 2004 by Neil Shubin and colleagues (N. H. Shubin et al., 2006).

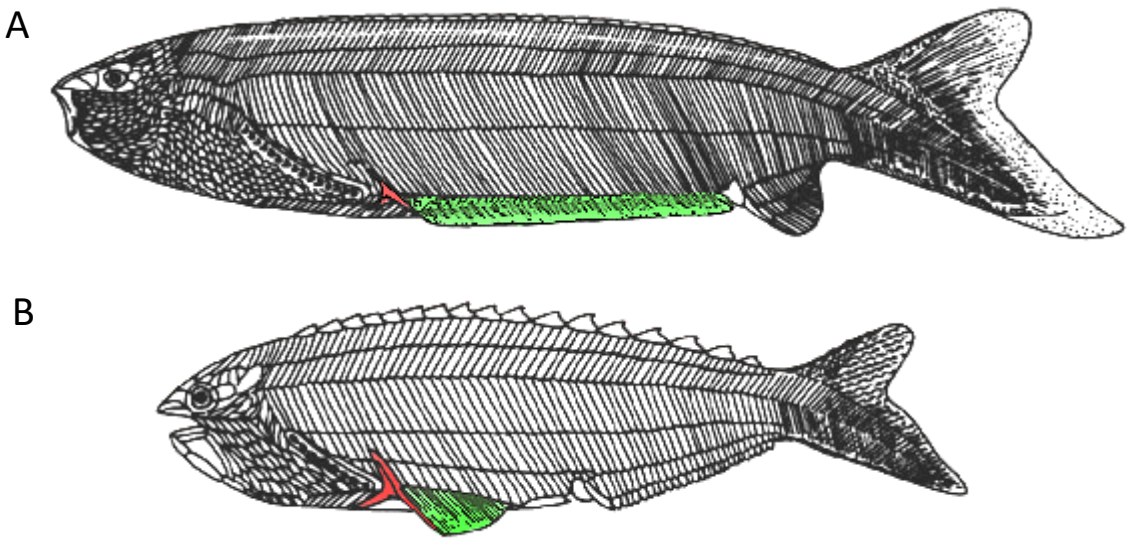

Figure 1.3 – Pharyngolepis (A) and Rhyncholepis (B), with a shorter pair of pectoral fins, adapted (Janvier, 1996).

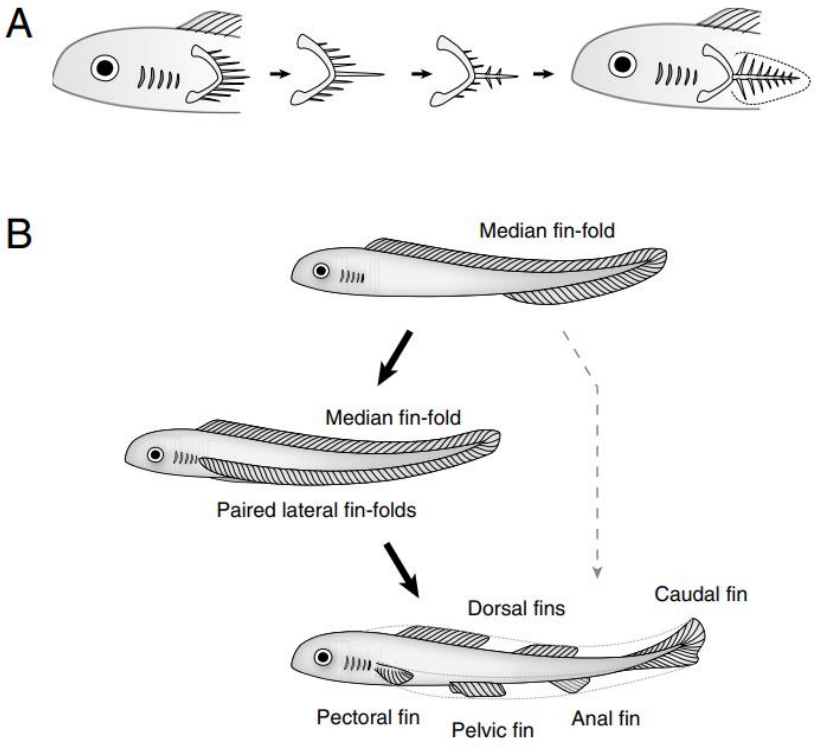

Figure 1.4 – The two theories that try to explain how the paired fins appeared. The gill arch theory (A) and the fin-fold theory (B), adapted (Pieretti et al., 2015).

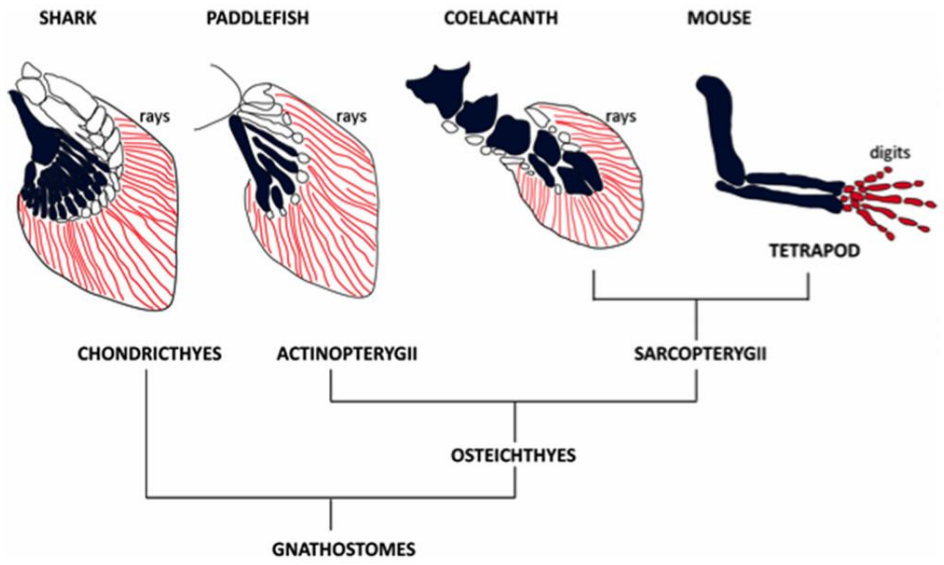

Figure 1.5 – Evolution of appendages, adapted (Paço & Freitas, 2018).

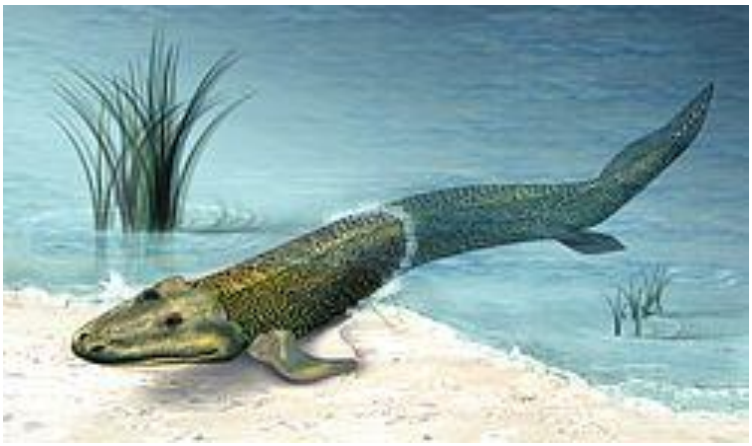

Figure 1.6 – *Tiktaalik roseae,* reconstruction from the National Science Foundation.

Evidence is very strong when suggesting that the Vertebrate limbs we know today derived from the fish fins, especially if we take in consideration the developmental data (Freitas et al., 2014). Anatomical studies show that, despite of the different aspects, all Vertebrate limbs have the same pattern of bones, namely a zeugopod, a stylopod and an autopod domain (Tamura et al., 2008). The process of formation of the limb bud is also very similar among different species of Vertebrates, suggesting strongly that this network is highly functional and, therefore, conserved in the evolutionary history of the limb.

Modulation of *Hox* genes expression, namely of *Hoxd13*, seems to be a key aspect that changed between fish fins to tetrapod limbs (Paço & Freitas, 2018). In this work, we are particularly interested in the identification of the molecular mechanisms associated with *Hoxd13* that might be behind the evolution in the so-called fin-to-limb transition in Vertebrates, the major event that propelled the colonization of land by this group.

1.3 Development of Vertebrate's limbs

Vertebrate´s limbs start to form by the continuous proliferation of a mass of cells from the LPM of the body wall, giving rise to 4 distinct buds, 2 pectoral and 2 pelvic, also known as forelimb and hindlimb in tetrapods (Zuniga, 2015). It seems that the identity of these appendages is

established even prior to their outgrowth from the LPM. In fact, if we transplant the LPM from the wing-forming region of a chicken, at early stages, the transplanted region will then develop a wing bud (Stephens et al., 1993; Tickle, 2015).

Throughout development, the limb bud has 3 areas important for the molecular signaling required for its outgrowth and patterning: the progress zone (PZ), the zone of polarizing activity (ZPA) and the apical ectodermal ridge (AER) (Fig. 1.7A) (Pignatti et al., 2014). All of them interact with each other and are focal for the correct development of the limb. As an example of the importance of these regions during limb development, if we remove the AER, for instance, the limb bud will stop growing (Haro et al., 2014).

These 3 components are also very important in the determination of the limb axial identity (Fig. 1.7B). Every appendage, whatever is it a fin, an arm, or a wing, has 3 principal axes; the proximal-distal axis from the trunk to the tip of the digits or fin rays; the anterior-posterior and the dorsal-ventral axis, which is particularly differentiated when observing the digits in tetrapods (Fig. 1.7B) (Das De & Sebastin, 2019). The formation of these structures requires the interaction between molecules produced in the PZ, ZPA and AER (Lin & Zhang, 2020).

When the embryo reaches the somitogenesis stage, a group of genes, known as the *Hox* clusters, start to be transcribed throughout the embryo (Fig. 1.8). Each gene from the cluster has restricted expression zones, and the encoded protein act as transcription factor in that domain, activating particular gene networks (Lappin et al., 2006). Thus, the *Hox* genes are thought to be main organizers of the genetic networks involved in embryonic development and differentiation (Luo et al., 2019). During limb development, they are expressed subsequently, according with their position within the cluster, a process known as “collinearity”.

It is thought that the antagonistic interaction between a proximal-to-distal gradient of retinoic acid (RA) and a distal-to-proximal gradient of fibroblast growth factors (Fgf) creates 3 distinct zones on the limb by controlling the expression of *Hox* genes from the A and D clusters; *Meis/HOX9-10* in the prospective stylopod, *HOX11* in the prospective zeugopod and *HOX13* in the prospective autopod (Fig. 1.8) (N. Shubin et al., 1997).

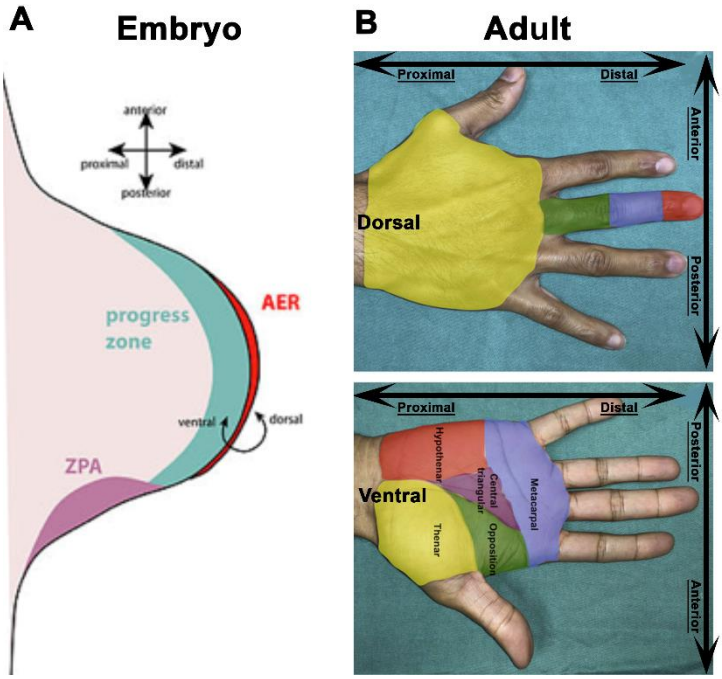

Figure 1.7: Limb regulatory regions and axes **A.** The three main regulatory regions of the limb bud during embryonic development, the ZPA, PZ and AER. Adapted (Te Welscher et al., 2002)**. B.** The limb axes particularly differentiated in the autopod (hand/feet). Adapted (Das De & Sebastin, 2019).

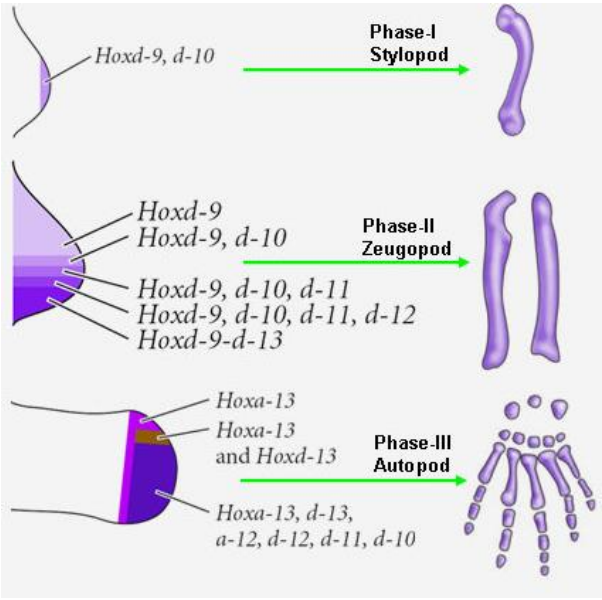

Figure 1.8: *Hox* gene expression during limb development. *Hoxd9* and *Hoxd10* are expressed in the newly formed limb bud, leading to the formation of the stylopod. Then, other *Hoxd* genes are collinearly expressed, leading to the formation of the zeugopod. Lastly, re- expression of 5'*HoxD* and *HoxA* genes, leads to the formation of the autopod. Adapted (N. Shubin et al., 1997) and modified by (Abbasi, 2008).

Apart from the proximal-distal differentiation, *Hox* gene expression is also important to define the antero-posterior axis during limb development. In that process, it is going to be equally important the expression of *Sonic hedgehog* (*Shh*) in the ZPA, the zone in the posterior margin of the limb bud that works as a signaling center (Lettice et al., 2003). The encoded protein diffuses throughout the limb, generating a gradient that influences gene expression (Tickle & Towers, 2017). The ZPA is where Shh is more concentrated, and the anterior region is where the concentration is lower. The expression of this gene is going to be also important for the patterning of the digits. *Shh* has a strong correlation with *Fgf* genes, as these interact with enhancer regions, leading to a more accessible or restricted DNA binding sites through acetylation (Peluso et al., 2017). Since *Fgf* are known targets of *Hox* genes, we can thus see the connection between *Hox* genes and *Shh* expression (Royle et al., 2021). The dorsal-ventral axis is regulated by two antagonistic mechanisms (the Wingless-related integrations site (Wnt) and the bone morphogenic proteins (BMP) signaling pathways). Wnt signaling will originate the dorsal side, while BMP signaling will regulate the formation of the ventral side. (Tarazona et al., 2019). BMP signaling is also very important in the formation of the digits (Pignatti et al., 2014). As BMP's are targets of the *Hoxd13* network (Salsi et al., 2008), we aimed to analyze several genes involved in this process, like down targets of BMP signaling, like Muscle Segment Homeobox genes (*Msx*), whose function is to regulate the interactions between the AER and the underlying mesenchyme (Hollnagel et al., 1999).

1.4 *Hox* genes and their role in the limb development

1.4.1 *Hox* genes

Hox genes are a subset of homeobox genes that are grouped in 4 clusters in the human genome: HoxA, chromosome 7, HoxB, chromosome 17, HoxC, chromosome 12 and HoxD in chromosome 2 (Fig. 1.9). These genes encode transcription factors containing a helix-turn-helix structure that binds to the DNA (homeodomain). Their main functions are gene expression regulation during embryonic development, being very important in the establishment of cell identity along the body axes.

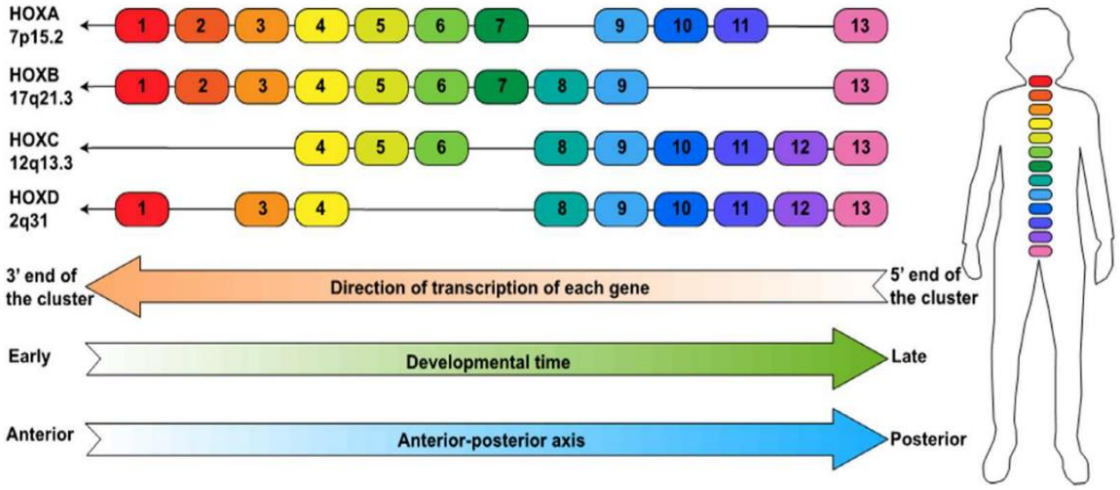

Figure 1.9 – *Hox* gene clusters in humans and their patterns of expression, adapted (Luo et al., 2019).

The number of Hox clusters present in an organism reflects the evolutionary history of its genome. Thus, a single Hox cluster is characteristic of the genomes of Invertebrates, inclusively the cephalochordates, such as the amphioxus. Then, in most Vertebrate lineages, the most common feature is four clusters that appeared due to two rounds of whole genome duplication (2WGDs) during evolution (Kuraku, 2011). Teleosts, such as the zebrafish, represent an exception within Vertebrates. This lineage suffered an extra whole genome duplication (3WGD) and, therefore, instead of 4 Hox clusters, they present 8 (Amores et al., 1998). However, several of the duplicated genes have been lost secondarily during teleost evolution, such as the *hoxd13b*. In addition, for the genes that remain duplicated, they seem to maintain often an equivalent activity (Bruce et al., 2001) or suffer "subfuncionalization" (Mateus et al., 2020).

Within the clusters, *Hox* genes are numbered from 1 to 13, but, as evolution progressed, some of the paralogs were lost, and, therefore, clusters do not have all the same number of genes. *Hox* genes are numbered from the 3' end to the 5' end of the cluster and their expression starts at the 3' end in the most anterior territories of the body axis. As development progresses, from an anterior to posterior direction, subsequent 5' *Hox* genes begin to be expressed and 3' ones start to be downregulated (Luo et al., 2019).

Since paralogs are so similar between them, both in sequence and structure, there is the possibility that, in case one of them is absent, the other one can overcompensate the missing gene by being overexpressed. An experiment with mice, that have 3 *Hox11* paralogs (*Hoxa11*, *Hoxc11* and *Hoxd11*), showed that if one *Hox11* is knockout (KO), the kidney forms normally, but if two *Hox11* paralogs are KO, the kidneys have hypoplasia. If the three paralogs are absent, the kidneys do not form at all and the embryo cannot survive (Wellik et al., 2002).

Besides, some other *Hox* genes involved in the formation of the limbs and digits can result in serious diseases in humans. For instance, heterozygous mutations in *Hoxa13* cause hand–foot–genital syndrome, whereas *Hoxd1*3 mutations result in malformations of fingers. In addition, aberrant expressions of some *Hox* genes have been also connected to particular cancer types, such as breast cancer in mammals (de Bessa Garcia et al., 2020).

Sánchez-Herrero (Sánchez-Herrero, 2013) and others have shown that Hox proteins are responsible for controlling the formation of structures and organs by regulating a variety of processes from cell division and death to cell morphology. These functions are probably achieved through the regulation of genes involved in these pathways. Here, we are interested in deciphering the mechanisms involved in the evolution of tetrapod limbs, which is intrinsically linked to the origin of the digits, and we will focus on the molecular networks associate to *Hoxd13*. Given that the function of these genes is tightly linked with the development of the digits, to unravel its targets and associated mechanisms can help to understand fundamental aspects of limb evolution, but also improve knowledge in digit malformations diseases and how to treat them.

1.4.2 *Hoxd13* network

Several studies have shown that *Hoxd13*, located at the 5' of the cluster, is deeply involved in the formation of the limb, but specially in the establishment of the autopod and digits (Beccari et al., 2021). *Hoxd13* is known to have two distinct waves of expression, both in fish as in tetrapods (Freitas et al., 2007). The first wave is very similar between Vertebrates, but the second wave is quite different, since it is more spatially-restricted in fish, as detected in shark, paddlefish and zebrafish. In tetrapods, however, *Hoxd13* expands its domain of expression (Fig. 1.10), and we

think that this alteration of expression might be related with the development of new structures that gave origin to the maintenance of the AER and formation of the limb (Freitas et al., 2014).

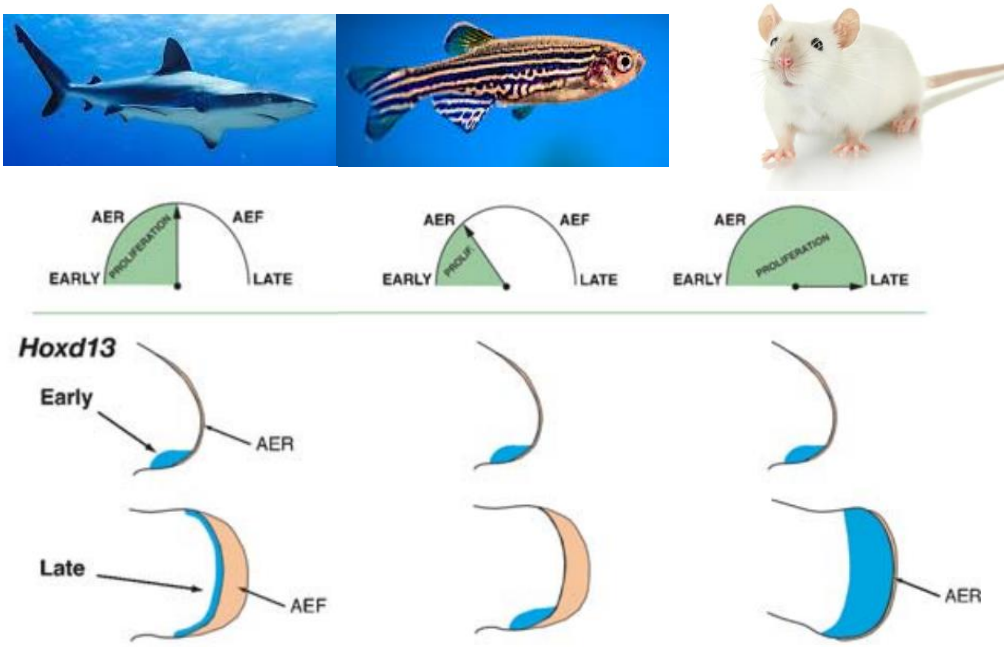

Figure 1.10 – *Hoxd13* gene expression in shark, zebrafish and tetrapod (Freitas et al., 2007).

Following this idea, the next step to understand how the limb developmental program was established in the tetrapod ancestors would be to study the underlying mechanisms associated to the *Hoxd13* targets (Fig. 1.11). Among them, *meis1* and *emx2*, responsible for proximal fin identity, *fbn1* and *dacha* genes, responsible for coordinating skeletogenesis, and BMPs (*bmp2b, bmp4, bmp7a and bmp7b*), *Fgf8* and *smoc2*, responsible for maintaining the AER and promote finfold outgrowth (Choi et al., 2012).

Freitas and collaborators have shown what happens to the expression of these targets when *hoxd13a* is upregulated during the development of zebrafish fins (Castro et al., 2021). In this work, we continue to study the mechanisms involved in fin development using zebrafish as a model in which we can mimic what happened during the fin to limb transition in terms of gene expression. This event mostly involved expansion and formation of more complex endoskeleton elements,

while also diminishing the distal ectodermal finfold, which is formed by elongation of the AER (Paço & Freitas, 2018).

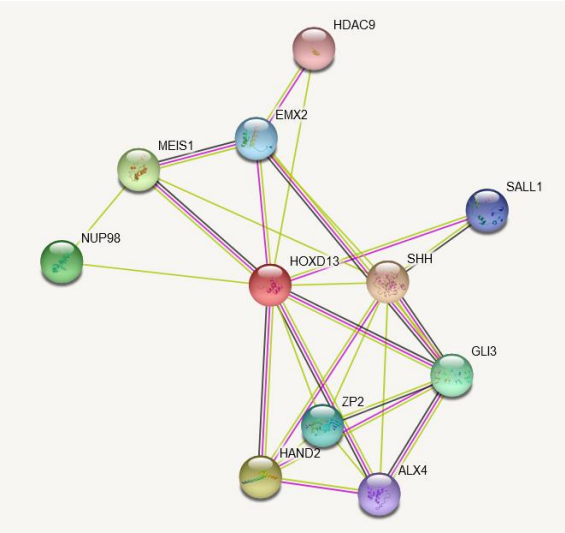

Figure 1.11 – *Hoxd13* gene network, by STRING (www.string-db.org).

1.5 Zebrafish: model organism to study molecularly the fin-to-limb transition

1.5.1 Characterization

Zebrafish (*Danio rerio)* (Fig. 1.12) is a teleost of small size, originated from the rivers of the northeast of India, and has already many applications as a model organism in both genetic and developmental studies (Dooley & Zon, 2000; Loucks & Ahlgren, 2012). Among its advantages to be considered a good model organism are its small size, the production of great amounts of fertilized eggs and a small-time lapse between egg and adulthood, about 3 months only. Besides, its genome and other basic features are already very well-known, and it is easy to manipulate and to adapt genetic and developmental techniques. Finally, the cost of maintaining a zebrafish facility is far lower compared to other Vertebrate models, such as the mice.

Having external fertilization, it is possible to observe the development of the embryos from the first stages, and, therefore, we can select which ones are viable and well formed, before proceeding

to the protocols, which can give more clear results in the end. Allied with the transparency of the egg, it is easy to genetically manipulate the embryos with microinjection techniques.

Figure 1.12 – *Danio rerio*, photo from "Memorial Sloan Kettering Cancer Center (www.mskcc.org).

Being a Vertebrate, zebrafish has evolutionary similarities with humans, and it can be used in diseases treatment studies, bearing in mind that we cannot directly extrapolate these results to humans, given that zebrafish does not have the same metabolic rates neither all tissues that human beings have (Dooley & Zon, 2000).

As the first animal to become a tetrapod like creature is thought to be a fish, the zebrafish can work as a model to identify ancestor mechanisms involved in the formation of the locomotory appendages and, using genetic manipulations, we can try to mimic the transition from fins to limbs. As a fish, it shares the same anatomical features that the ancestor of tetrapods should have had; 2 pectoral and 2 pelvic fins that evolved to the forelimb and hindlimb, respectively. Because all the above described and the extensive genetic and developmental knowledge of this organism, zebrafish was chosen as the model for our study.

1.5.2 Fin development

The zebrafish fin is composed of two different types of skeletal elements. Looking at the proximal part of the fin, it is formed by cartilage and mineralized bone, responsible for supporting the muscle masses and nerves (endoskeleton). Contrary, in the more distal part of the fin, ossified structures named lepidotrichia and actinotrichia are present, the first being segmented ossified soft

fin-rays, while the second ones are formed by collagen and non-collagen components (exoskeleton) (Fig. 1.13) (Grandel & Schulte-Merker, 1998).

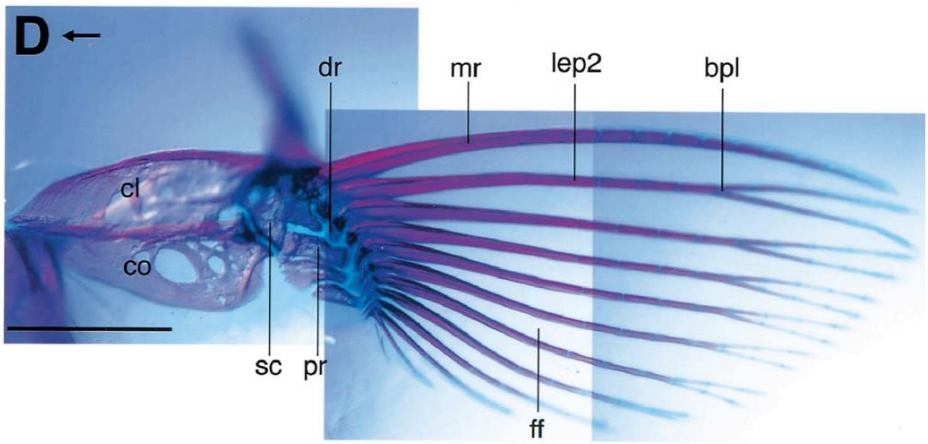

Figure 1.13 – *Danio rerio* fin bone morphology (bpl, first branchpoint of lepidotrichs; co, coracoid; cl, cleithrum; dr, distal radials; ff, finfold; lep, lepidotrich; mr, marginal ray; pr, proximal radials; sc, scapula), adapted (Grandel & Schulte-Merker, 1998).

In these species, as in all known tetrapods, the appendages start with the proliferation of mesodermal tissue, from the LPM that starts growing out of the trunk. As so, the fin bud is covered in ectodermal tissue, which start to thick at the distal border, giving rise to the AER. It is in this structure that appears the first difference in the formation of a fin in comparison with a limb. In tetrapods, the AER is maintained until the formation of digits and controls a variety of networks related to this process (Towers, 2018). However, in fishes in general, including in the zebrafish, the AER is transformed into a finfold, where the exoskeletal of the fin is formed from mesenchymal cells that migrate into it, starting approximately at 48 hours post-fertilization (hpf). The endoskeleton is formed at earlier stages, around 36 hpf, from the mesodermal cells' differentiation, and gives rise to a cartilaginous disc, observed at 56 hpf clearly. Pelvic fins form much later, during the third week of development, at 18 days post-fertilization (dpf) and form directly adult fin structure (Grandel & Schulte-Merker, 1998).

1.5.3 Involvement of *Hoxd13* in fin-to-limb modifications

Freitas and colleagues have already shown the effects that differential expression of *hoxd13a* causes in the finfold of zebrafish (Castro et al., 2021; Freitas et al., 2012). When this gene is overexpressed, the finfold size is greatly reduced. In contrast, long finfolds in zebrafish mutants (*Lof*^{dt2}) are associated with lower expression of this gene, when compared to the wild-type (*wtAB*) condition at the same developmental stages. Some other conclusions were drawn from these studies, namely that the expression levels of *bmp2b* and *casp3* also vary on zebrafish lines presenting distinct finfold sizes associated with distinct levels of *hoxd13a* expression.

In this study, our aim was to understand the networks associated to *hoxd13a* and its putative targets that could direct the transformation of the finfold with the final aim to understand the mechanisms involved in the fin-to-limb transition. For that purpose, we used three conditions with different *hoxd13a* expression levels: *wtAB* with normal finfold, *hoxd13a:hsp70* transgenic line with truncated finfold, and *Leo*^{t1}*/Lof*^{dt2} with long finfold.

1.5.4 Involvement of BMP signaling in fin-to-limb modifications

One of the putative targets found to be influenced by *hoxd13a* modulation in our previous assays was *bmp2b* (Castro et al., 2021). We found that this gene is upregulated after *hoxd13a* overexpression in zebrafish line *hoxd13a:hsp70* characterized by truncated finfolds, and that the overexpression of *bmp2b* led to a similar phenotype. Therefore, we hypothesized that the BMP signaling may have a major role in the definition of the finfold size. In agreement with our idea, Pizzete and colleagues found that the AER is negatively regulated by the BMP signaling, as inhibition of BMP led to AER maintenance and finfold elongation (Pizette & Niswander, 1999b). To test this hypothesis, we investigated the expression levels of several genes involved in the BMP signaling in the three lines above indicated, namely *bmp2b, msx1b* and *msx2b,, smoc1, smoc2, noggin3* and *gremlin1a* (Mateus et al., 2020) as well as *smad1,* a molecule involved in the activation of the BMP signaling cascade.

2. MATERIALS AND METHODS

2.1 Fish maintenance and manipulation

Zebrafish experiments followed European Union (EU) Animal Research Guidelines and the experimental design was approved by the Ethics Committee of IBMC/I3S and DGAV (Portugal). Three distinct lines were used: *wtAB*; mutant *Leo*^{t1}/*Lof*^{dt2} and transgenic *hoxd13a:hsp70*. Individuals were kept in tanks in an animal facility where all the major abiotic factors are controlled: light, temperature, and water conductivity. Water is recirculated through a system (Tecniplast-Zebtec) that maintains temperature at 26ºC and pH 6,7-7.0. The room temperature and light cycles are also controlled. Tanks are clean every day and fish are fed 3 times a day. The number of individuals per 3L tank was inferior to 28 fish, according with current EU guidelines for animal welfare.

Adult fish were used only with the purpose to generate embryos, which served two major roles: 1) develop until a specific time point and then be collected to use in different experiments or 2) develop until adulthood and become progenitors.

Embryos were subjected to a process of lixiviation before being placed in the tanks within the water system. When embryos reached 24 hpf, they were immersed successively in the following solutions: NaOH, H_2O, NaOH, H_2O and H_2O.

2.1.1 Reproduction, egg collection and embryo selection

The embryos used on this study were obtained from in-breeding of adults from the same line, to control genetic variability. To obtain the eggs, adult fish were put in a smaller reproduction tank (Fig. 2.1) which had a gride on the bottom, avoiding egg predation by the progenitors. It also had a removable barrier dividing the tank in half, which allows the separation of males and females, usually in rates of 1:2 or 2:3 respectively. In the morning after the separation of males and females, this barrier was removed, and water was withdrawn until it reached a shallow level. The tank was then kept under a fluorescence light for at least 20 minutes. These conditions mimic the natural environment of this species during mating.

Figure 2.1 – Scheme of a reproduction tank with all the attachments.

Lastly, the eggs were collected using a net and put in a petri dish containing E3 solution, a medium that avoids fungi proliferation and that includes 300 µL of methylene blue and 10 mL of 100x E3. The plates rested in an incubator at 28,5°C, where 1 hour of time corresponds to 1 hpf, according to Kimmel (Kimmel et al., 1995). Besides, according to the same author, the temperature can be manipulated in order to accelerate or retard the development time. In here, we used the temperature of 32°C to reach the 86hpf, one of the stages that we evaluated, after only 72 hours.

2.1.2 Heat shock treatment

Prior to the heat shock treatments, at 24hpf, we confirmed that the embryos were transgenics, searching for green fluorescent signal in the hearth under the stereoscope. This signal

is due to the activation of the cmlc2 promoter associated to the reporter gene EGFP, also present in the construct (Freitas et al., 2012) (Fig. 2.2).

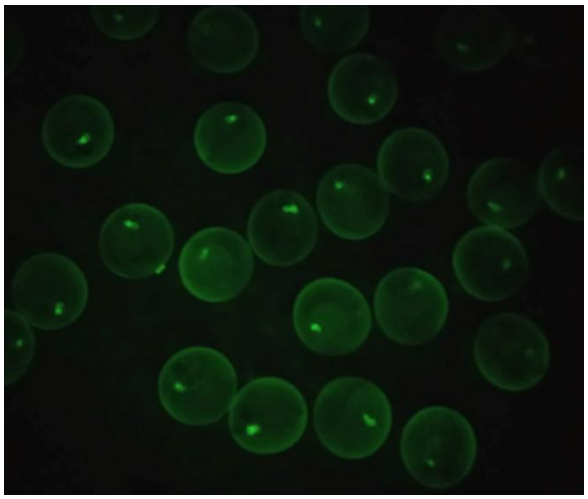

Figure 2.2 – Photography of *hoxd13a:hsp70* under a scope with GFP filter, showing the "bleeding heart" effect that distinguishes the ones that are able to overexpress *hoxd13.*

It is known that the second wave of expression of 5' *Hox* genes in zebrafish starts at 30hpf (Ahn & Ho, 2008) and it has been suggested that the reinforcement of this wave by new enhancers during evolution may have triggered the fin-to-limb transition (Freitas et al., 2012). Knowing that, the heat shock was first performed at that time point in order to increase *hoxd13a* expression during the second wave and mimick the levels of expression during tetrapod limb development. To maintain these high levels of expression during fin development, subsequent heat shocks were given to the embryos every 24 hours, starting at 48hpf. The treatment consisted in immersing the embryos, within tubes, in E3 medium at 38,5 ºC during 1 hour. Afterwards, embryos returned to petri dishes with E3 solution at 28,5ºC and were kept in the incubator until the next heat shock, dissection, or fixation. Prior to these proceedings, we selected the embryos with the expected phenotype (truncated finfolds) and we confirmed that the controls did not present this characteristic.

2.1.3 Fixation and dehydration of embryos

When the embryos reached the developmental stages that we aimed to analyze through *in situ* hybridization (ISH) protocols, we fixed them in 4% PFA (paraformaldehyde) overnight at 4ºC. In the next day, they were passed through a series of increasing methanol concentration. Each passage had the time of 5 minutes and was done on ice and in the shaking platform, following the order: PBT 100% (PBS (phosphate buffered saline) 1x with 0.1% Tween-20), MeOH (Methanol) 25% / PBT 75%, MeOH 50% / PBT 50%, MeOH 75% / PBT 25% and 2 washes in MeOH 100%. Lastly, dehydrated embryos were stored at -20ºC, in order to preserve their RNA content. This dehydration step also makes embryos more permeable to the riboprobes used in the ISH.

.

2.2 *In situ* hybridization

2.2.1 Riboprobes' acquisition

We solicited the plasmids containing the DNA fragments required for riboprobe synthesis to other labs that sent them in filter paper. We used an online platform to find these labs that already performed good quality ISH with each of the riboprobes, the ZFin-Org website. The paper was cut with scissors and put inside a microcentrifuge tube and the DNA was eluted with the addition of 50 µL of water RNA/DNA free for 5 minutes. Then, the tubes were centrifuged at low speed for 30 seconds. The plasmid in the supernatant was recovered to a new tube and stored at -20ºC or immediately used in a PCR of 25 µL final volume.

2.2.2 Polymerase chain reaction (PCR)

PCR is a technique that allows the amplification of DNA fragments of interest into thousands of millions of identical copies, often used in quantitative and qualitative analysis. It starts with the denaturation of the DNA through high temperatures (60ºC) that breaks the hydrogen bonds between nucleotides and split the double chain into 2 single strands, allowing for specific primers to bind to them and then allow their replication by the action of a DNA polymerase, which occurs through 25-35 cycles.

2.2.3 Agarose gel electrophoresis

This technique relies in a difference of electrical potential applied to a solid matrix gel. The current established attracts DNA molecules to the cathode, forcing them to pass through the matrix, where they get separated by size/weight. Bigger molecules stay closer to the wells, while smaller fragments travel faster in the gel and stay far from the wells. In our experiments, we used a 2% agarose gel in tris-acetate-EDTA (TAE) buffer. We ensured dissolution of the agarose in the TAE using a microwave to heat the mix. Then, we let the mix cool down and added 2µL of Safe-Green (NZYTech) to dye the nucleic acids. Then, the mix was placed in a gel support with combs that created space for the wells and let it polymerize at room temperature (RT). Finally, we dove the gel in TAE 1x and add 5µL of PCR product with 1µL of loading dye 6x to each well. In the first well, we placed 3µL of DNA Ladder 100 Bp (NZYTech) that allowed to know the approximate size of our fragments. The run was at 100 V and the gel was lastly checked under UV light.

2.2.4 DNA template amplification

After confirmation of PCR amplification of the plasmid by agarose gel electrophoresis, we re-amplify the DNA obtained performing another PCR, this time to get 4x50 µL of product. We used M13F/M13R primers, as they successfully amplified the fragment of the plasmid that contained the DNA fragment required for the synthesis of the riboprobe. The reaction was performed accordingly to the manufacturers of the enzyme, as referred in Table 2.1. In Table 2.2 are listed the temperatures used in the thermocycler.

We confirmed again this amplification by agarose gel electrophoresis. We then cleaned and concentrated the DNA fragments using the "DNA Clean & Concentrator^{TM}-5" kit (ZYMO). First, we mixed 5 volumes of "DNA Binding Buffer" with 1 volume of DNA samples in a 1,5 mL microcentrifuge tube and mixed briefly by vortexing. Then, we transferred the mix to a "Zimo-Spin Column" in a "Collection Tube", centrifuged for 30 seconds between 10,000 – 16,000 x *g* and discarded the flow-through. Afterwards, we added 200 µL of "DNA Wash Buffer" to the column, centrifuged 30 seconds at the same x *g* and repeated. Finally, we added ≥ 6 µL (20 µL) of "DNA Elution Buffer" or water (we used water) to the column and incubated 1 minute at RT, transferred it to a 1,5 mL microcentrifuge tube and centrifuged at the same x *g* for 30 seconds to elute the

DNA. We then measured DNA concentration and quality in a NanoDrop quantification machine (ND-1000 spectrophotometer, "software" ND-1000 V3.1.2, Nanodrop Techonologies). This ultra-pure DNA can be used immediately or stored at -20ºC.

Components	25 µL	50 µL	Final Concentration
10x PCR Buffer, -Mg	2,5 µL	5 µL	1x
5 mM $MgCl_2$	0,75 µL	1,5 µL	1,5 mM
10 mM dNTP mix	0,5 µL	1 µL	0,2 mM each
10 µM forward primer	0,5 µL	1 µL	0,2 µM
10 µM reverse primer	0,5 µL	1 µL	0,2 µM
Template DNA	varies	varies	<500 ng
Platinum™ *Taq* DNA Polymerase	0,1 µL	0,2 µL	2 U
Water, nucleasse-free	to 25 µL	to 50 µL	-

Table 2.1 – PCR reagents and concentrations for "Invitrogen™ Platinum™ *Taq* DNA Polymerase" kit according to manufacturer's instructions.

Step	T ºC	Time	Cycles
Initial Denaturation	95 ºC	3 min.	1
Denaturation	95 ºC	30 seg.	30
Primer Annealing	62 ºC	30 seg.	
Extension	72 ºC	1 min.	
Final Extension	72 ºC	5 min.	1

Table 2.2 – PCR protocol with steps, T ºC, time and number of cycles. The temperature for the primer annealing step needs to be adjusted for the used primers annealing temperature.

2.2.5 *In vitro* transcription

To obtain the riboprobe for ISH, we needed to transcribe the DNA fragment with an RNA polymerase and to find a way to "read" where the probe was going to be in the embryo. For that, we used a synthetic RNA fragment called Dig-UTP, which consists of a digoxigenin (DIG) molecule bond to uridine 5'-triphosphate. As so, this nucleotide will be introduced by the RNA

polymerase whenever an adenine is transcribed from the DNA sequence, instead of an uracil. By applying a specific antibody for digoxigenin conjugated with an alkaline phosphatase (anti-Dig-AP) we could detect where the RNA of interest is being transcribed in the embryo by a color reaction, blue in this case. The *in vitro* transcription occurred at 37ºC for at least 2 hours (mix in Table 2.3) followed by a DNase I digestion, at 37ºC for 30 minutes, to remove the remaining DNA. The RNA polymerases vary according to the orientation of the DNA fragment in the plasmids in order to obtain an anti-sense riboprobe (Table 2.4).

Components	**25 µL**	**Final Concentration**
10x transcription buffer	2,5 µL	1x
DTT 0.1M	2,5 µL	1,5 mM
DIG-RNA labelling mix (UTP)	2,5 µL	0,2 mM each
Ribolock RNase inhibitor (40U/µL)	2 µL	0,2 µM
RNA polymerase (20U/µL)	2 µL	0,2 µM
Linear template DNA	10 µL	<500 ng
H_2O DEPC	3,5 µL	2 U

Table 2.3 – *In vitro* transcription mix used to obtain the RNA probes.

Gene	**Riboprobe**	**RNA polymerase**	**Intitution**
bmp2b	Anti-sense	T3	Toulouse University, France
msx2a	Anti-sense	T3	Klinikum University, Germany
msx2b	Anti-sense	T7	
msx2d	Anti-sense	T3	

Table 2.4 – *In vitro* transcription used RNA polymerases, genes studied and the institution that conceded the plasmid with the probe.

Afterwards, we run a PCR with the samples followed by an electrophoresis agarose gel to confirm RNA production and DNA absence and we proceeded to the RNA probe purification step. Here, we used "mini Quick Spin Columns" (Roche). First, we resuspended the column matrix and removed the top cap and the bottom tip. Then, we placed it in a microcentrifuge tube and centrifuged at 1,000 x *g* for 1 minute, to pack the column, and discarded the residual buffer. Next, the sample was applied to the center of the column, which was centrifuged at 1,000 x *g* for 4

minutes to recover the eluate with the purified RNA probe. Lastly, we measured the RNA amount and quality in the NanoDrop quantification machine (ND-1000 spectrophotometer, "software" ND-1000 V3.1.2, Nanodrop Techonologies).

2.2.6 *In situ* hybridization (ISH)

This technique is used to detect specific RNA fragments, utilizing complementary RNA probes derived of *in vitro* transcription of cloned DNA fragments (riboprobes). The riboprobes were labeled with digoxigenin (DIG), which works as a reporter, since it reacts with the substrate that is formed when complementary molecules bind, giving the location of expression of the target gene. We used 5 embryos per condition and *actinodin1* riboprobe (*and1*) as a positive control for the *in situ* reaction, since it is a strong marker of the finfold area. The protocol has the duration of 3 days and was adapted from Thisse (Thisse & Thisse, 2008).

Day 1 started with the rehydration of the embryos, where they are passed through a series of MeOH/PBT solutions with increasing concentrations of PBT, following the order: 25% PBT / 75% MeOH, 50% PBT / 50% MeOH, 75% PBT / 25% MeOH and finally 2 washes in 100% PBT. Embryos stayed in these solution 5 minutes on ice and in shaking platform. Afterwards, embryos were treated with proteinase K during a period that has been established per stage (Table 2.5). The proteinase K digestion was stopped with two washes during 5 minutes in PBT on ice on the shaking platform, and refixation of embryos in 4% PFA for a minimum of 20 minutes at RT. Then, the PFA was removed with 3 washes in PBT, during 5 minutes on ice and shaking. After that, embryos were immersed in hybridization mix containing yeast tRNA (Hyb+) (Table 2.6) at 70ºC for at least 2 hours.

Lastly, we removed Hyb+ from embryos, added Hyb+ with the designated probe and leave overnight at 70ºC for at least 16h.

Stage of development (hpf)	Digestion time with proteinase K (minutes)
Early somitogenesis	1
Late somitogenesis	3
24	5
36/38	7
48 *	10
72/96	15
120 *	20
144 *	20
168 *	20

Table 2.5 – Time (in minutes) for the proteinase K digestion according to the developmental stage of the embryos (hpf). *Times verified and optimized for probes staining the finfold.

	Stock Concentration	For 100 mL HM	Final Concentration	
Heparin		5 mg	50 µg/mL	Hyb+
tRNA (yeast RNA)	50 mg/mL	1 mL	500 µg/mL	Hyb+
Formamide		50-65 mL	50-65%	Hyb-
SSC	20x	25 mL	5x	Hyb+
Tween20	25%	400 µL	0.1%	Hyb-
Citric acid	1M	920 µL	0.0092M	Hyb-
MQ		to 100 mL		Hyb-

Table 2.6 – Hyb+ and Hyb- constitution. Store both solutions at -20 ºC and adapt the percentage of formamide according to the desired stringency. We used 50% for Hyb+ and 65% for Hyb-.

At day 2, most solutions were pre-heated at 70ºC for 10 minutes prior to use. The first wash was with the hybridization mix without yeast tRNA (Hyb-) (Table 2.6) and then with saline sodium citrate (SSC) solutions, an acid salt buffer solution used for its buffering capacity that increases stringency. The washing process is at 70ºC and was performed as follow: 100% Hyb- (brief wash),

75% Hyb- / 25% 2xSSC, 50% Hyb- / 50% 2xSSC, 25% Hyb- / 75% 2xSSC and 100% 2xSSC, at 70ºC and 10 minutes each. Then 2x30 minutes washes with 0,05xSSC at 70ºC. Afterwards, 2x5 minutes 50% 0,05xSSC / 50% PBT at RT and finally 2x PBT 5 minutes at RT. Then, we made a blocking solution consisting of 2% bovine serum albumin (BSA), 2% Goat Serum and PBT, where the embryos and the antibody for the DIG (Anti-DIG) were incubated at RT and ice, respectively, both on shaking, for at least 2h. After that time, we removed the blocking solution from the embryos, added the blocking solution with antibody and incubated at 4ºC overnight, protected from light and in shaking.

In day 3, embryos were washed in PBT at RT, shaking, 4x30 minutes, followed by a 15 minutes wash with AP- (without $MgCl_2$) and 2x10 minutes AP+ (with $MgCl_2$) (Table 2.7). In this last step, we found that doing the AP+ incubation 1x10 minutes and 1x30 minutes gives faster color reaction.

Then, we prepared the color solution with NBT/BCIP (3,4µL NBT/mL and 3,5µL BCIP/mL of AP+) in AP+ and incubated embryos in a ceramic plate, shaking and in dark. Every 15 minutes, we monitored under the stereoscope, and, once it reached proper staining in the finfold, we gently washed embryos in PBT 2x2 minutes in the dark and fixed them in 4% PFA for at least 1 hour. Lastly, we replaced the 4% PFA with 80% glycerol in PBS. The embryos were kept there for at least 24h and then the fins were dissected under the stereoscope, cover-slipped and photographed under the microscope (40X amplification).

Components	Volume (for 100mL of AP+)
1M Tris HCl pH 9.5	10 mL
1M $MgCl_2$	5 mL
5M NaCl	2 mL
Tween 20 (just prior to use, it spoils)	100 µL
H2O MQ	To 100 mL

Table 2.7 – AP+ components. AP+ should be used immediately after, so we need to do new AP+ for each *in situ* protocol, according to the volume needed. For AP-, simply do not add $MgCl_2$. AP- can be stocked at RT and used in posterior protocols.

2.3 Real-Time Quantitative Polymerase Chain Reaction (RT-qPCR)

RT-qPCR is a technique derived from the classical PCR that allows for the detection and quantification of products amplified in each PCR cycle, due to the incorporation of a fluorescent molecule in the reaction (Edwards et al., 2005).

2.3.1 RNA extraction

To extract the RNA in order to obtain cDNA, we first dissected the embryo portion containing the fins (around 50 fish per condition) at stages 24hpf, 32hpf, 48hpf, 56hpf, 72hpf, 86hpf, 96hpf and 120hpf. Embryos were first dechorionized and anesthetized with tricaine. Finally, we submerged the dissected pieces in RNA Later (Fisher), which preserved the RNA of tissues at -20ºC. Afterwards, we proceeded to homogenize the mixture using a homogenizer machine.

To extract the RNA from the homogenized mix we centrifuged at 4ºC, 12 000 x *g*, 1 hour and discarded the supernatant. Then, we added 400µL of trizol to the pallet, vortexed and centrifuged at 4ºC, 12 000 x *g* for 2 minutes (afterwards, can be kept overnight at 4ºC if necessary). Next, the mix incubated 10 minutes at RT, and we added 80µL of chloroform and briefly vortexed the mix. Then, we centrifuged, this time at 4ºC, 12 000 x *g* for 15 minutes and collected the aqueous phase (without trizol) to a new tube. Afterwards, we added 200µL of isopropanol and let the mix incubate at RT for 10 minutes, followed by yet another centrifuge step, at 4ºC, 12 000 x *g* for 15 minutes and discarded the supernatant. Later, we resuspended the pallet in 400µL of 75% ethanol, vortexed the mix, centrifuged at 4ºC, 10 000 x *g* for 5 minutes and discarded the supernatant. We resuspended the pallet one more time in 150µL of 75% ethanol, vortexed and repeated the previous centrifuge step. Lastly, we let the pallet dry at RT for 15 minutes by letting the cover of the tube open, we resuspended in 25µL of water DNase/RNase free and incubated at 60ºC for 5 minutes, gently mixed and incubated for more 5 minutes. At this time, we had an RNA and DNA extract mixture, so we performed a DNAse I digestion, as indicated in Table 2.8, which involved an incubation at 37ºC for 1 hour, followed by 2 minutes in ice.

Finally, we needed to precipitate the RNA to separate it from the mix. To that end, we added sodium acetate pH=4,6 to a final concentration of 0,2M and 2,5x volume of 100% ethanol, homogenized through inversion and let it precipitate overnight at -20 ºC. In the next day, we

centrifuged at 4ºC, 10 000 rpm for 30 minutes and discarded the supernatant. We resuspended the pallet in 150 µL of 75% ethanol, vortexed briefly and centrifuged at 4ºC, 10 000 rpm for 10 minutes. Then, we added another 150 µL of 75% ethanol, homogenized through inversion, without resuspending the pallet, and centrifuged again, repeating the last step. Then, we took out as much supernatant as possible and let it dry at RT for 15 minutes at least, with the cover open. Lastly, we resuspended in 25 µL of H_2O DNase/RNase free and measured the amount of RNA obtained in a NanoDrop machine. This RNA was used immediately for cDNA conversion or stored at -80ºC until further usage.

Components	Volume
RNA mixture	All
Buffer 10x $MgCl_2$	3 µL
DNase I	1 µL
H_2O RNase free	6 µL

Table 2.8 – DNase digestion mix to clear any remaining DNA from the RNA solution.

2.3.2 RNA conversion to cDNA

RNA was converted into cDNA that was then used in PCR methods. cDNA synthesis was performed to obtain 500 ng for each sample, using the mix in Table 2.9 that included the "High Capacity cDNA Reverse Transcription Kit" (Thermo Fisher Scientific). The thermocycler program used to perform the conversion is in Table 2.10. DNA production was then confirmed by PCR reaction for *β-actin2* and electrophoresis gel.

Components	Volume
RNA	To 500 ng
Buffer 10x	2 µL
25x dNTP	0,8 µL
10x random primers	2 µL
Multisense 20x	1 µL
Ribolock RNase inhibitor	0,5 µL
H_2O	To 20 µL

Table 2.9 – Mix used to convert RNA into cDNA.

Temperature (ºC)	Time (min.)
25	10
37	120
85	5
4	Until removal

Table 2.10 – Program for the RNA to cDNA conversion.

2.3.3 RT-qPCR reaction

RT-qPCR is a technique derived from the classical PCR that allows for the detection and quantification of products amplified in each PCR cycle, due to the incorporation of a fluorescent molecule in the reaction (Edwards et al., 2005). We used SYBR Green, an intercalator agent that binds to the DNA. We used the program "Bio-Rad CFX Manager" to analyze the raw data and "Excel" to compile them and calculate relative gene expression differences. The graph resulting from this reaction gives a curve of amplification with 3 major phases: basal, exponential, and stationary. At first, the amount of PCR product is not high enough for the fluorescence to be detected by the reader, so the graph line is low. Around 16-18 cycles (for *β-actin2*), the amount of DNA produced is high enough to be detected, and grows exponentially until the reagents cease to exist, and so the reaction cannot continue, and the fluorescence signal reaches a plateau (around 28-30 cycles). The exponential phase is used to measure relative expression of genes due to its more accurate representation of the PCR reaction quantification (Fig. 2.3) (Kubista et al., 2006).

We calculated the relative gene expression, using a reference gene to compare with our gene of interest expression levels (Edwards et al., 2005). For the quantification, we consider the first cycle of the exponential phase (Ct) and compare the thresholds between the gene of reference and our gene of interest. This value of Ct corresponds to the number of cycles necessary to detect the fluorescence.

The reference genes are normally independent from the gene network that is being analyzed and are constant throughout development. In our case, we used *β-actin2*, after evaluating several others that were less stable throughout zebrafish fin development. The gene of interest and the reference are always measured in triplicates, so that we have three technical replicates. To have biological replicates, we confirm the results of the first RT-qPCR test with a second one. Afterwards, we normalize the target gene to our reference gene, normalized all samples to 24hpf

of each line and did a separate comparison between stages. The data is exploited using the software Bio-Rad iQ5 Optical System Software Version 2.0 and submitted to statistical treatment using unpaired *t-test* and ANOVA test in the GraphPad Prism software, to determine if samples were statistically different from each other. The quantification is calculated in the Excel with the $2^{-\Delta\Delta Ct}$ method (Kubista et al., 2006).

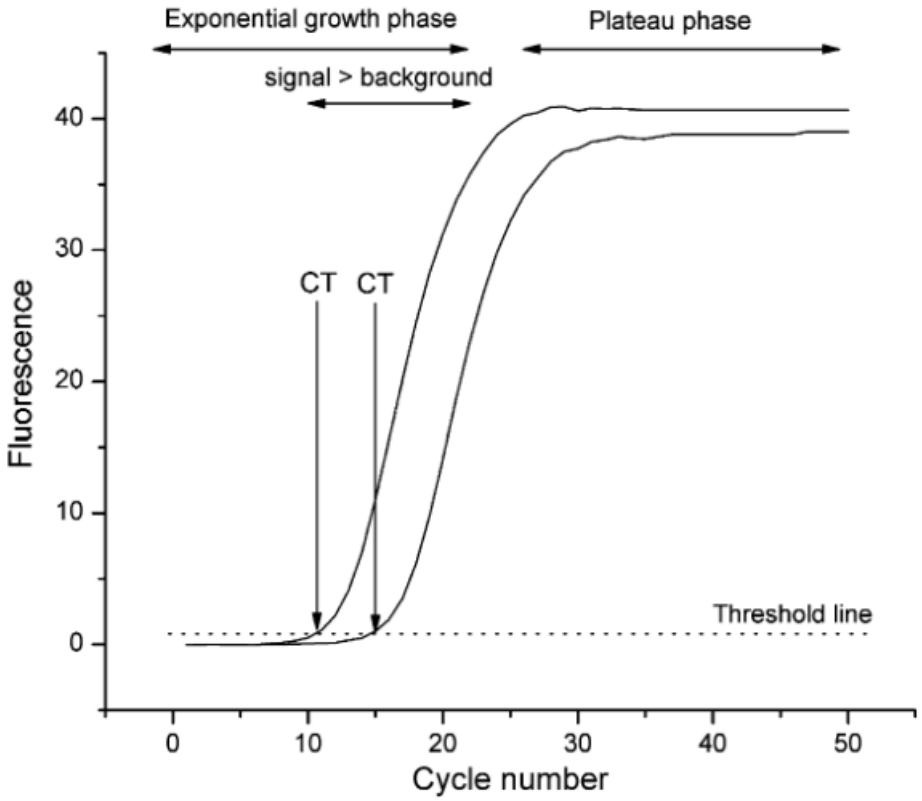

Figure 2.3 – Representation of the curve obtained in RT-qPCR reaction with the different phases and the Ct values used for further calculations (Kubista et al., 2006).

3. RESULTS

3.1. Long-fin *Leo^{t1}/Lof^{dt2}* mutants develop longer embryonic finfolds

In this project, we aimed to compare molecular mechanisms involved in the formation of three distinct embryonic finfolds in the following zebrafish linages: *wtAB (Wt)*; transgenic *hoxd13a:hsp70;* and mutant *Leo^{t1}/Lof^{dt2}*. Regarding the transgenic line, we already knew that, after *hoxd13a* overexpression, the finfold stops to elongate and, therefore, it is much shorter than the *Wt* (Freitas et al., 2012). However, it was not known if the finfold of *Leo^{t1}/Lof^{dt2}* mutants was indeed more elongated than in the *Wt* condition**,** as suggested by the size of the fin-rays in the adults (Fig. 3.1A). Here, we pursued the analyses already initiated in the lab that intended to evaluate the development of the finfold in this mutant in comparison with the *Wt* (Fig. 3.1B). To this end, we performed ISH at particular developmental stages using a riboprobe that marks the finfold: *actinodin1 (and1)* (Zhang et al., 2010), which was published in (Castro et al., 2021). The *and1* encodes a non-collagenous protein that is a major component of the actinotrichia, the first exoskeletal elements formed during fin development (Lalonde et al., 2016).

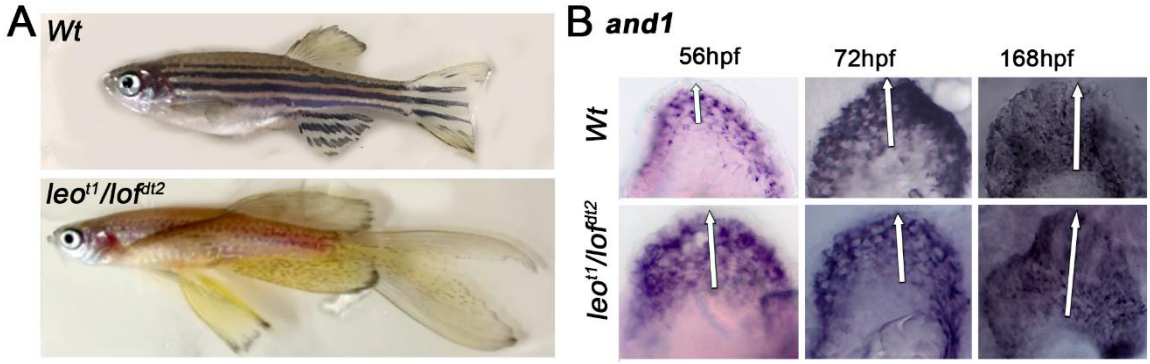

Figure 3.1: Finfold growth in leo^{t1}/lof^{dt2} mutants and controls (*Wt*). **A.** Fin phenotype comparisons in adults. **B.** Finfold size comparison during development evaluated after *and1* ISH, published *in* (Castro et al., 2021).

3.2 Expression of *bmp2b* relates to finfold size in the distinct lineages

Data from our lab have suggested that the shortening of the finfold in transgenics overexpressing *hoxd13a* was associated with increased levels of *bmp2b* and that a higher quantity of its transcripts similarly causes shortening of the finfold (Castro et al., 2021). In addition, it was also demonstrated that the transgenic fins had higher expression of a gene related to the apoptotic process (*casp3*). Regarding Leo^{t1}/Lof^{dt2} mutants, the previous work in the lab also suggested that, at stage 86hpf, these animals express less *hoxd13a* in their developing fins in comparison with the *wtAB*.

Here, we contributed to characterize the expression of *bmp2b* during fin development in Leo^{t1}/Lof^{dt2} mutants, taking the opportunity to evaluate the levels of expression of genes indicative of apoptosis (*casp3*) and proliferation (*ccnb1*). Our data suggested that, at 86hpf, the expression of *bmp2b*, *casp3,* and *ccnb1* was lower than the control (Fig. 3.2), which was published in (Castro et al., 2021).

We then evaluate the expression of *bmp2b* at earlier stages in the three conditions by ISH. This analysis suggests that, as early as 56hpf, while *wtAB* and Leo^{t1}/Lof^{dt2} fins have low *bmp2b* expression, it is visible in the truncated finfold of *hsp70:hoxd13a* fins (Fig. 3.3). Here, we were also able to detect persistence of *bmp2b* expression at 72hpf in the finfold of transgenic fins, while the *wtAB* have shown much lower levels detectable by ISH (Fig. 3.4). Taken together, our data is consistent with our hypothesis, suggesting that increased levels of *bmp2b*, mediated by *hoxd13a* transcription factors, may have been an important mechanism involved in the shortening of the finfold during evolution probably interfering with the apoptotic process in the finfold.

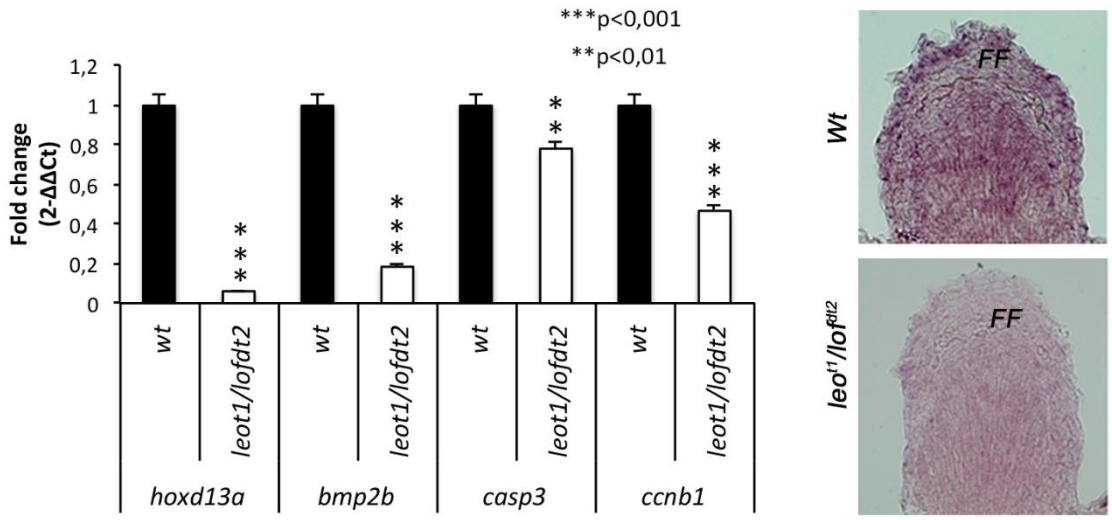

Figure 3.2: Gene expression analyses at 86hpf by RT-qPCR (on the left) and ISH (on the right), suggesting lower expression levels for *hoxd13a* and *bmp2b* in *leo*^{t1}*/lof*^{dt2} fins in comparison with *Wt* controls (***p<0,001), which was accompanied by decreased expression of *casp3*, involved in apoptosis (**p<0,01) and *ccnb1*, involved in proliferation (***p<0,001). Statistical significance evaluated by unpaired t-test, published *in* (Castro et al., 2021).

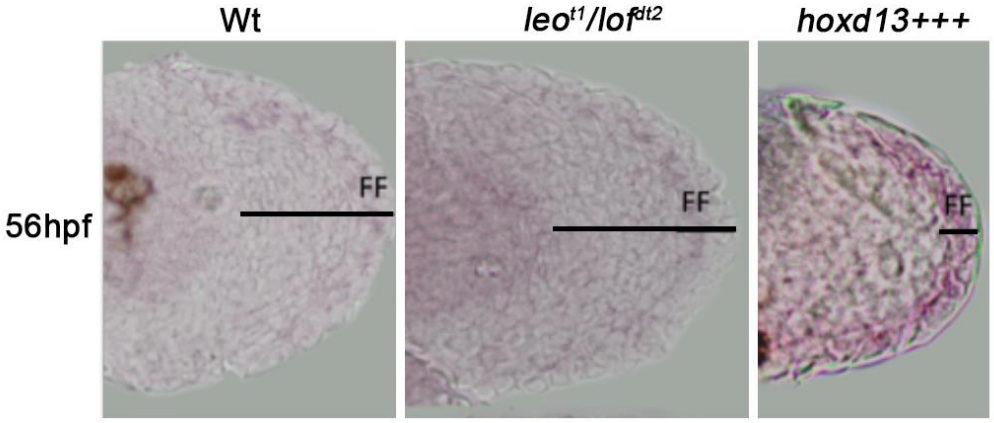

Figure 3.3: *bmp2b* expression evaluated by ISH at 56hpf in wild-type fins (*Wt*), *leo*^{t1}*/lof*^{dt2} with longer finfolds (FF), and *hsp70:hoxd13a* with shorter finfolds (*hoxd13*+++). Note marked expression in the truncated finfold of the transgenics (*hoxd13*+++), which is undetectable in the other lines.

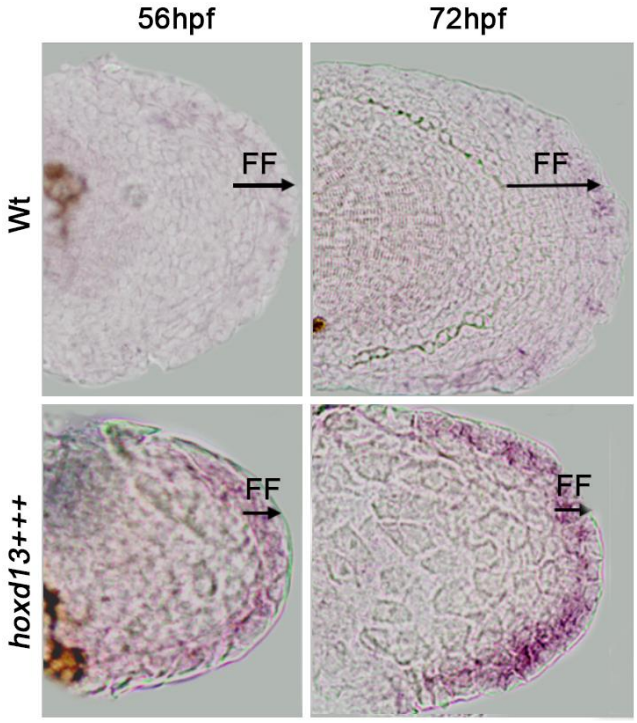

Figure 3.4: Comparison of the *bmp2b* expression evaluated by ISH at 56hpf and 72hpf in wild-type fins (*Wt*) and *hsp70:hoxd13a* with shorter finfolds (*hoxd13*+++). Note marked expression in the truncated finfold of the transgenics (*hoxd13*+++), which is in much lower levels in the *Wt*.

3.3 *bmp2b* expression dynamics are distinct in the three lineages analyzed

Pignatti and colleagues (Pignatti et al., 2014) investigated the dynamics of BMP activity in mouse limb mesenchyme and found that it fluctuates throughout development (Fig. 3.5). In an initial phase of BMP activity, it is high and important for the establishment of the AER (Fig. 3.5A). Then, it diminishes over time, a process that was related to the activation of the networks responsible for the patterning. (Fig. 3.5B). Finally, the BMP activity increases again, which is thought to trigger the exit of the cells to chondrogenesis (Fig. 3.5C). In addition, several studies have addressed the function of the BMP signaling in the ectodermal portion of the limb bud, proposing a role in inhibiting the elongation of the AER and promoting the development of the digits in the underlying mesenchyme (Choi et al., 2012; Pizette & Niswander, 1999a).

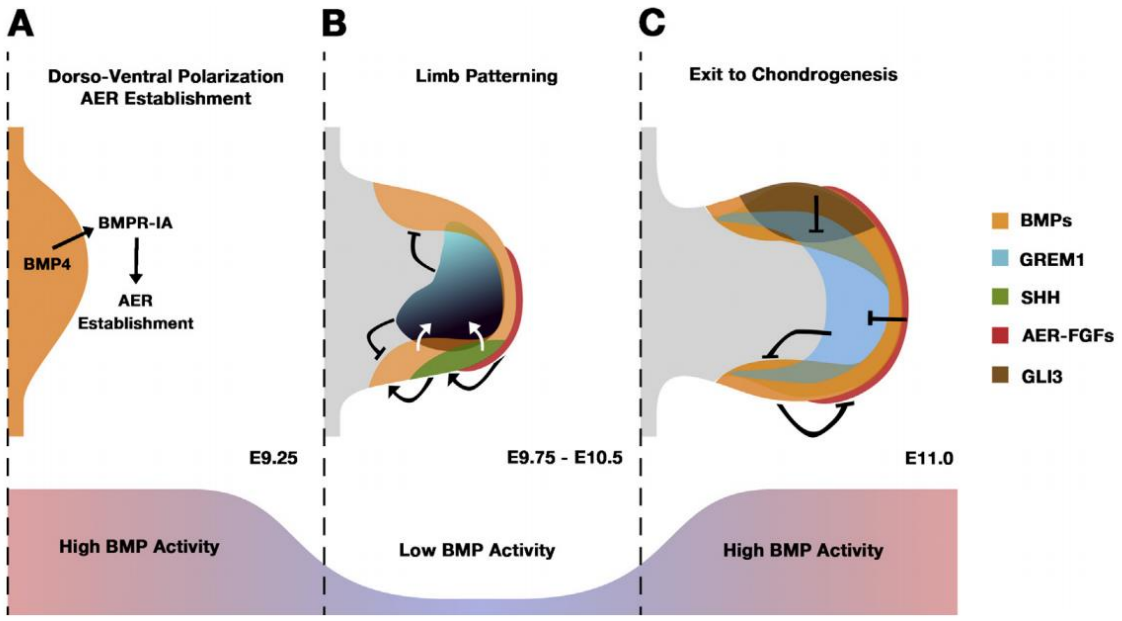

Figure 3.5: Dynamic of BMP activity during mice limb development. **A.** Limb bud initial outgrowth and establishment of the AER. **B.** Limb patterning. **C.** Exit of the mesenchymal cells to chondrogenesis. Adapted (Pignatti et al., 2014).

After accessing the differences in *bmp2b* expression in zebrafish lines with distinct embryonic finfolds, we next asked how different the dynamics of *bmp2b* expression throughout the development of their fins are. To this end, we prepared a collection of cDNAs from dissected fins at distinct developmental stages and performed RT-qPCR analyses for several genes involved in the BMP signaling. We decided to start our analyses at 24hpf because the transition between an AER and a finfold occurs in zebrafish at 34-36hpf (Grandel & Schulte-Merker, 1998) and, at that stage, most of the primordia of the endoskeleton is already formed (endoskeleton disc). Therefore, we assumed that most of the differences observed in the BMP dynamics were more related to finfold development after that time point.

Our results suggest that fluctuations in *bmp2b* expression also exist during the formation of these appendages, but they are variable according to the line (Fig. 3.6). In the *wtAB*, the *bmp2b* expression starts to diminish subtly after 24hpf and then increases at 72hpf and drops again at 86hpf. We hypothesized that, as it happens in the limb mesenchyme prior to the formation of the endoskeleton (Pignatti et al., 2014), we might have a first peak of *bmp2b* expression that might be

associated with the transition of the AER to the finfold, followed by a reduction of its levels that might be associated with a stage governed by patterning mechanisms. Later, the expression levels increase again at 72hpf, which is clearly visible in the finfold distal margin (Fig. 3.4), and that may relate to a stage in which cells are exiting towards differentiation.

Regarding the *Leo*^{t1}*/Lof*^{dt2} fins, the same downward trend on *bmp2b* expression is detectable, but just after 48hpf (Fig. 3.6). Also, in the graphs where we normalized all samples to each stage in each condition, it seems that *Leo*^{t1}*/Lof*^{dt2} (Fig. 3.7A) have lower levels of expression of *bmp2b* in general, associated with a larger finfold phenotype as we proposed in (Castro et al., 2021).

In the transgenics overexpressing *hoxd13a* (*hoxd13+++*), we detected a peak of expression at 32hpf that we suggest being associated with the heat shock treatments (Fig. 3.6 and Fig. 3.7B). That reinforces our hypothesis that *hoxd13a* triggers the *bmp2b* expression causing finfold truncation (Castro et al., 2021). However, we were not expecting that through the remaining development, the level of *bmp2b* would remain lower than the *wtAB*. We thought that maybe some compensatory mechanisms try to compensate the overexpression of *bmp2b*, due to the heat shock, and that these are responsible for the decrease in expression verified at 56hpf, in an attempt to reach normal levels of expression, which may not happen because we keep boosting the level of *bmp2b* with successive heat shocks, as the compensatory mechanisms try to repress it.

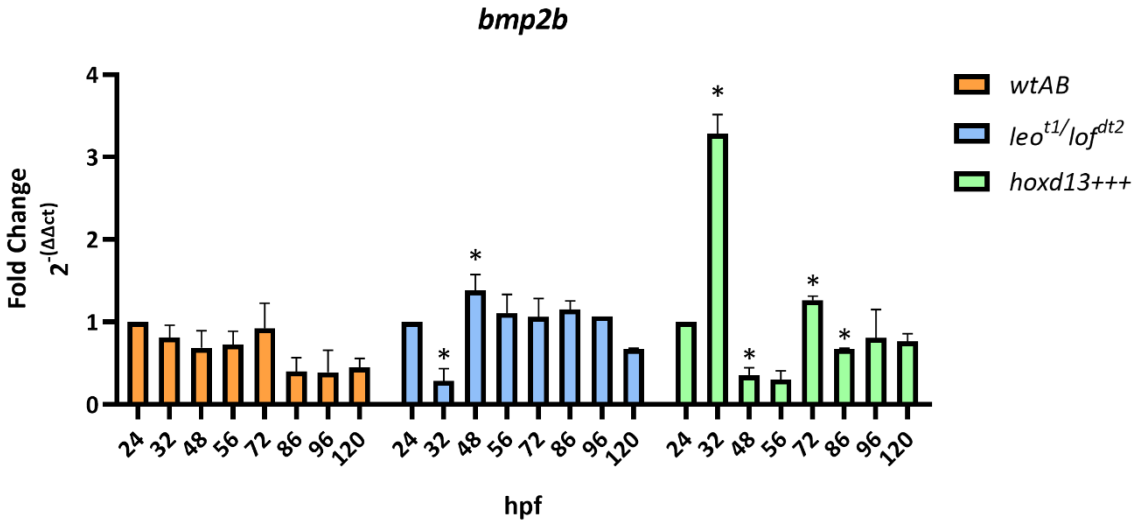

Figure 3.6: Dynamics of *bmp2b* expression by RT-qPCR throughout fin development in wild-type (*wtAB*), *leo*^{t1}*/lof*^{dt2} with longer finfolds, and *hsp70:hoxd13a* with shorter finfolds (*hoxd13+++*). Note the downward trend of *bmp2b* expression in the *wtAB* with two peaks, one at 24hpf and the other at 72hpf. Note also the same downward trend in *leo*^{t1}*/lof*^{dt2} fins starting after 48hpf. *´s represent the statistical significance between the designed stage and the previous one. These differences were calculated with a one-way ANOVA test, with p. value < 0.05.

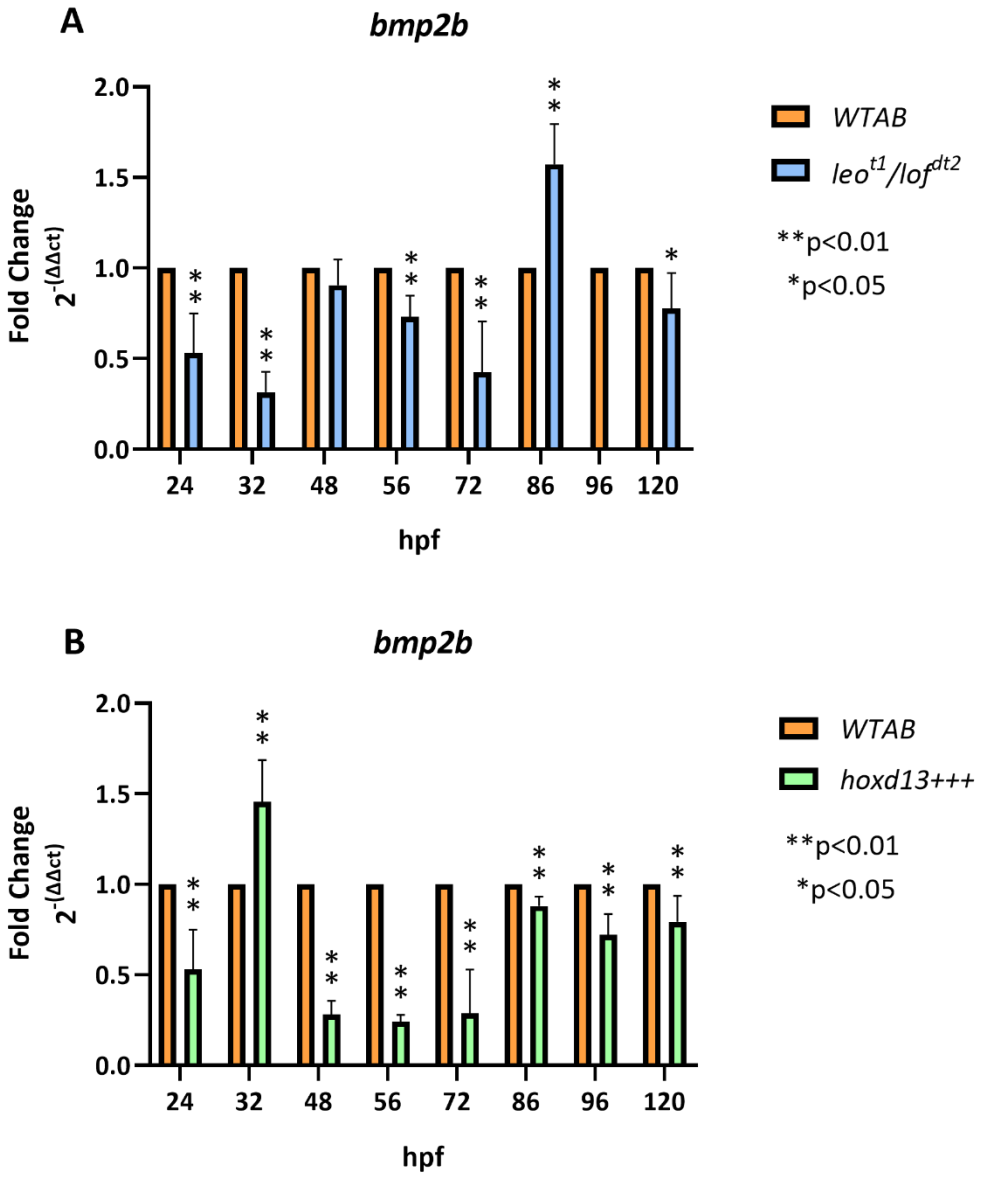

Figure 3.7: Comparison of *bmp2b* expression by RT-qPCR throughout fin development in wild-type (*wtAB*), *leo*^{t1}*/lof*^{dt2} with longer finfolds, and *hsp70:hoxd13a* with shorter finfolds (*hoxd13*+++). Note that *leo*^{t1}*/lof*^{dt2} presents a tendency to have fewer levels of expression, with a peak at 86hpf. The line *hsp70:hoxd13a* has a peak at 32hpf, due to the heat shock, and maintains a lower expression afterward. Data analyzed with *t-test*, with p. value < 0.01 or <0.05.

3.4 Expression dynamics of other genes involved in the BMP signaling

BMP signaling plays a crucial role in development and adult tissue homeostasis (Wang et al., 2014), and, in this work, we suggest that its modulation may have a function in the definition of the finfold size in fish. Moreover, we favor a hypothesis in which BMP signaling modulation, triggered by *Hoxd13* up-regulation during evolution, may have been involved in the transition from fish fins to tetrapod limbs.

Apart from *Bmp2*, many other molecular players are components of the BMP signaling, which can be either canonical or non-canonical depending on the involvement of Smad proteins (Fig. 3.8). In the canonical signaling pathway, BMP proteins initiate the signal transduction cascade by binding to cell surface receptors (BMPr). Bmp2 preferentially binds to type I receptors and recruits type II receptors (De Caestecker, 2004). This allows phosphorylation of the immediately downstream substrate proteins: Smad1, Smad5, and Smad8. These phosphorylated Smads (PSmad1/5/8) then associate with Smad4 and translocate to the nucleus acting as transcription factors.

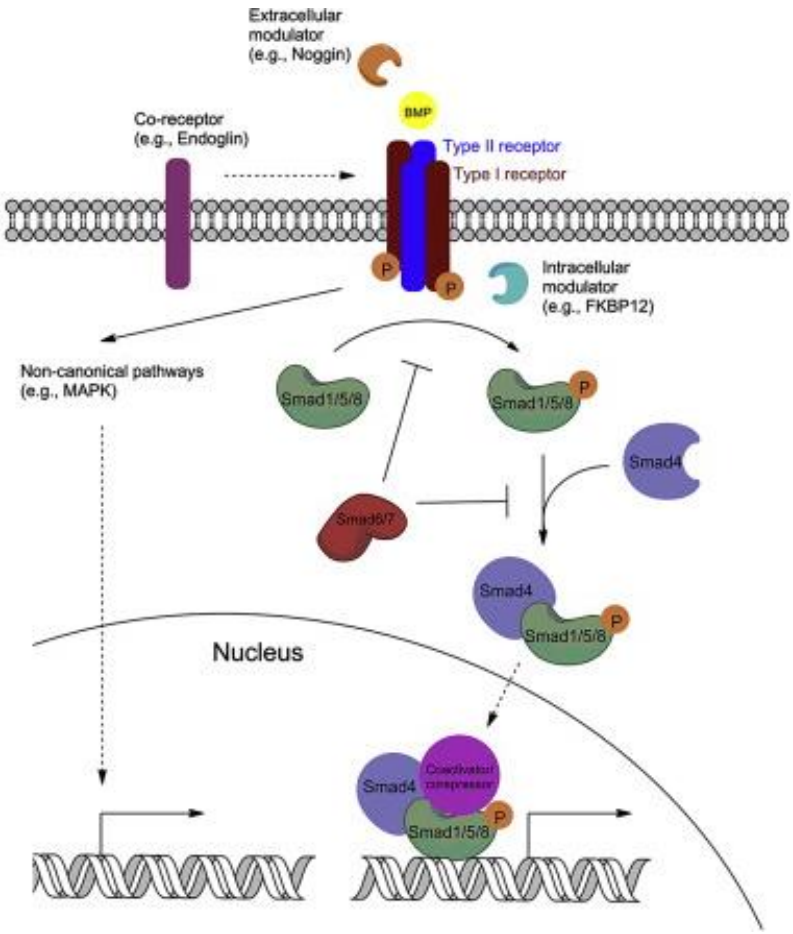

Figure 3.8: BMP family and signaling pathways, in (Wang et al., 2014).

3.4.1 Expression of *smad1*

To evaluate if the levels of *hoxd13a* in the three distinct lines can also be related with the expression levels of other components of the BMP signaling, we next evaluated the expression levels of *smad1* (Fig. 3.9 and Fig. 3.10).

In the *wtAB* fins, *smad1* and *bmp2b* have different dynamics of expression (Fig. 3.9). Regarding Leo^{t1}/Lof^{dt2} mutants, the expression of *smad1* seems to be similar in comparison with the *wtAB* (Fig. 3.10A), since the differences are not statistically significant.

In the transgenic fins, contrary to *bmp2b,* we found a decrease in *smad1* expression after the induction of *hoxd13a* overexpression, at 32hpf. Also, similarly with *bmp2b,* the expression drops at 56hpf and then starts to increase at 72hpf (Fig. 3.9) being, however, lower than in the *wtAB*

(Fig. 3.10B). These fluctuations may be related with compensatory mechanisms activated in the cells in the presence of enhanced BMP signaling. To try to compensate for the higher levels of *bmp2b* induced transcripts, the cells reduce the number of molecules necessary to continue the pathway. Both zebrafish lines have a peak at 96hpf in comparison to *wtAB.*

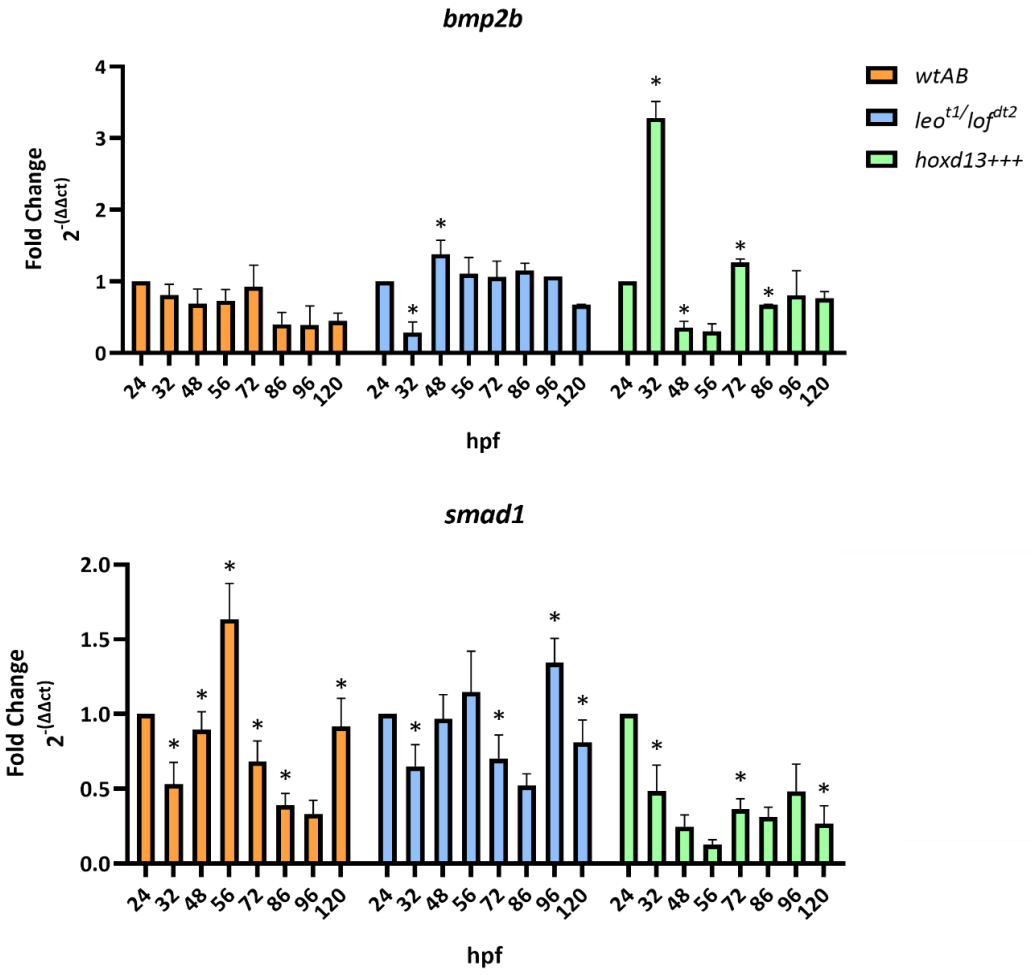

Figure 3.9: Expression dynamics of *bmp2b* and *smad1* during fin development (RT-qPCR) in wild-type (*wtAB*), *leo*^{t1}*/lof*^{dt2} with longer finfolds, and *hsp70:hoxd13a* with shorter finfolds (*hoxd13*+++). Note the accented fluctuations of *bmp2b* expression in the *wtAB* with a peak at 56hpf. In *leo*^{t1}*/lof*^{dt2} fins, the fluctuations seem less severe, and in the transgenic line it is clear a down expression of *smad1* in the peak of *bmp2b* at 32hpf. *´s represent the statistical significance between the designed stage and the previous one. These differences were calculated with a one-way ANOVA test, with p. value < 0.05.

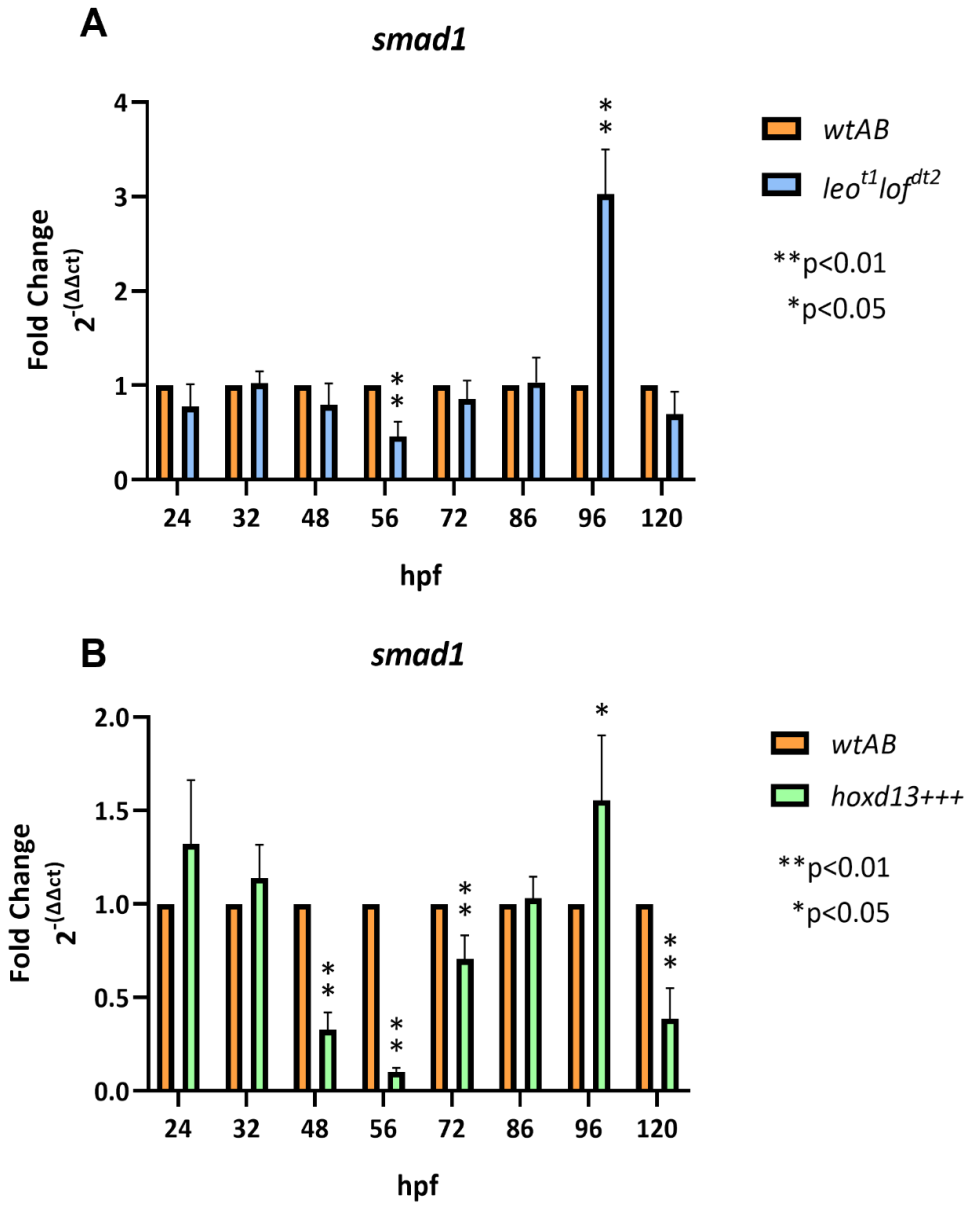

Figure 3.10: Comparison of *bmp2b* and *smad1* expression in fin development (RT-qPCR) in wild-type (*wtAB*), *leo*^{t1}*/lof*^{dt2} with longer finfolds, and *hsp70:hoxd13a* with shorter finfolds (*hoxd13*+++). Note that *leo*^{t1}*/lof*^{dt2} present almost no differences, despite a peak at 96hpf. The line *hsp70:hoxd13a* has a peak at 96hpf also and shows lower expression levels at other stages after the heat shock, suggesting a compensatory mechanism. Data analyzed with *t-test*, with p. value < 0.01 or <0.05.

3.4.2 Expression of BMP antagonists

To explore how BMP antagonists may play a role in the BMP signaling dynamics during the development of fins with distinct finfold size, we analyzed their expression in the lines considered in this study. We accessed the expression of *smoc1*, *smoc2*, *noggin3* and *gremlin1a* antagonists.

3.4.2.1 *smoc1* and *smoc2*

For *smoc1* and *smoc2* (Fig. 3.11) we found a dynamic of expression very similar with the one found for *bmp2b* in the three lines analyze: in the *wtAB*, we also detected a subtle downregulation from 24hpf to 56hpf and then a peak of expression at 72hpf (Fig. 3.11); in the Leo^{t1}/Lof^{dt2} line there are 2 peaks, at 48hpf and 86hpf for both *smoc* genes; in the *hoxd13a*-overexpressing condition, a peak of expression was detected at 32hpf, which is immediately after the heat shock treatment. This could be an attempt to downregulate the levels of *bmp2b* expression, using its antagonists, or it could be resultant from a direct impact of *hoxd13a* overexpression, suggesting that *smoc* genes could also be controlled by *hoxd13a*.

The coincident dynamics between the expression of *bmp2b* and *smoc1/smoc2* is consistent with recent findings suggesting that *Smoc* genes may regulate the BMP signaling during zebrafish fin development (Mateus et al., 2020). In addition, to our knowledge, this is the first indication that *Hoxd13* may act on the regulation of BMP agonists/antagonists during fin/limb development.

Interestingly, when comparing stages between lines (Fig. 3.12), we found out that the longer finfold condition has higher expression levels of *smoc* genes then the *wtAB* condition (Fig. 3.12A,B), that could be related with lower levels of its antagonist *bmp2b*. We suggest that this may corelate with stages in which the inhibition of the BMP signaling is being promoted to allow the additional outgrowth of the finfold observed in the mutant condition. In the transgenic line, however, the levels of expression of *smoc* genes are very similar to the *bmp2b* ones, all having a decrease at 48hpf that is maintained through most of the remaining development (Fig. 3.12C,D). Taking in account our working hypothesis, we suggest that this corresponds to stages in which BMP signaling is being promoted in the finfold, conducting to reduction of *smoc* genes expression. Thus, our data suggests that with higher levels of *smoc* genes, the finfold elongates (mutant line)

and, in contrast, when lower levels of *smoc* genes are present, the finfold is truncated (transgenic line).

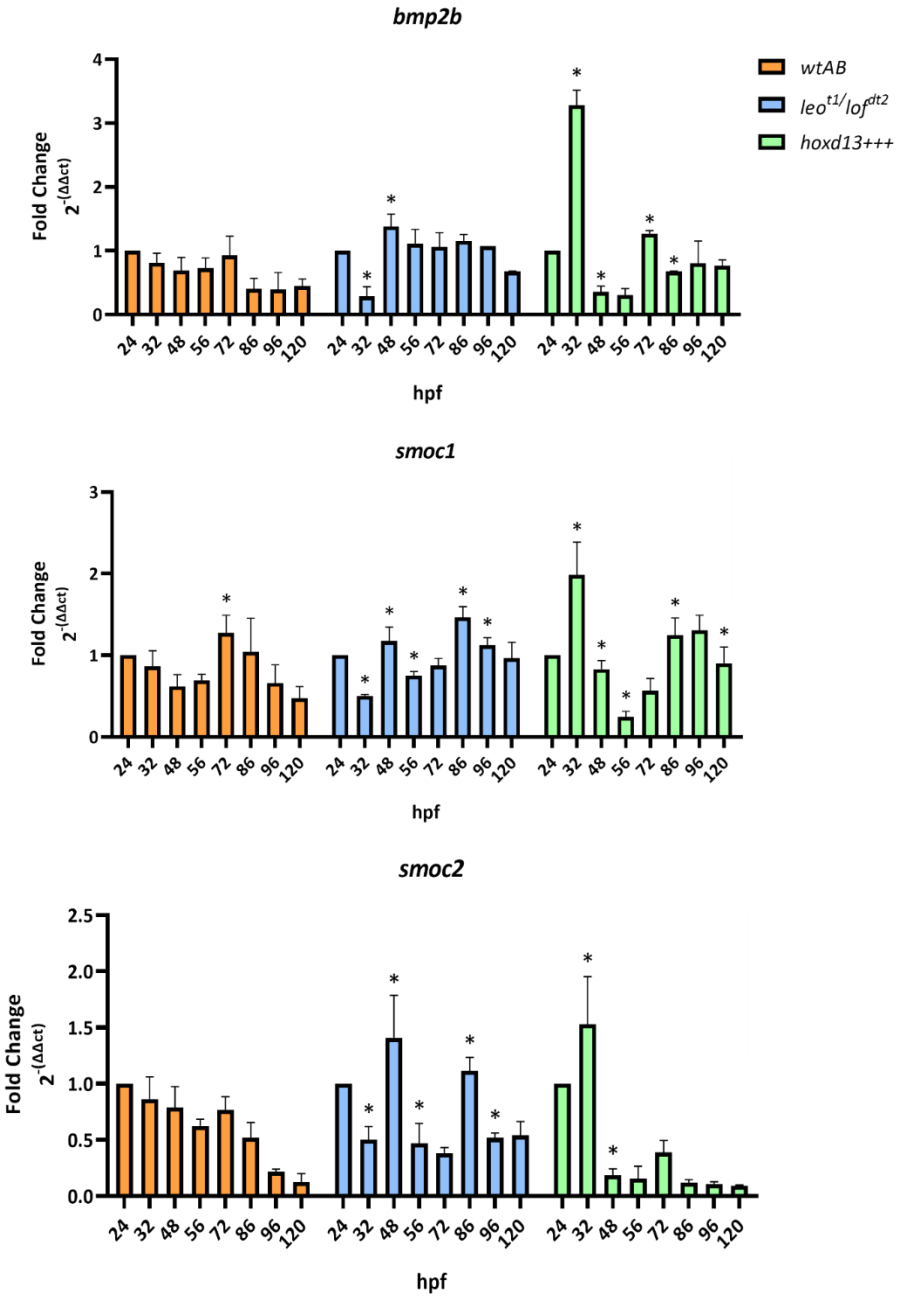

Figure 3.11: Dynamics of *bmp2b*, *smoc1* and *smoc2* during fin development (RT-qPCR) in wild-type (*wtAB*), *leo*^{t1}*/lof*^{dt2} with longer finfolds, and *hsp70:hoxd13a* with shorter finfolds (*hoxd13*+++). Note the very similar expression dynamics of the three genes. *´s represent the statistical significance between the designed stage and the previous one. These differences were calculated with a one-way ANOVA test, with p. value < 0.05.

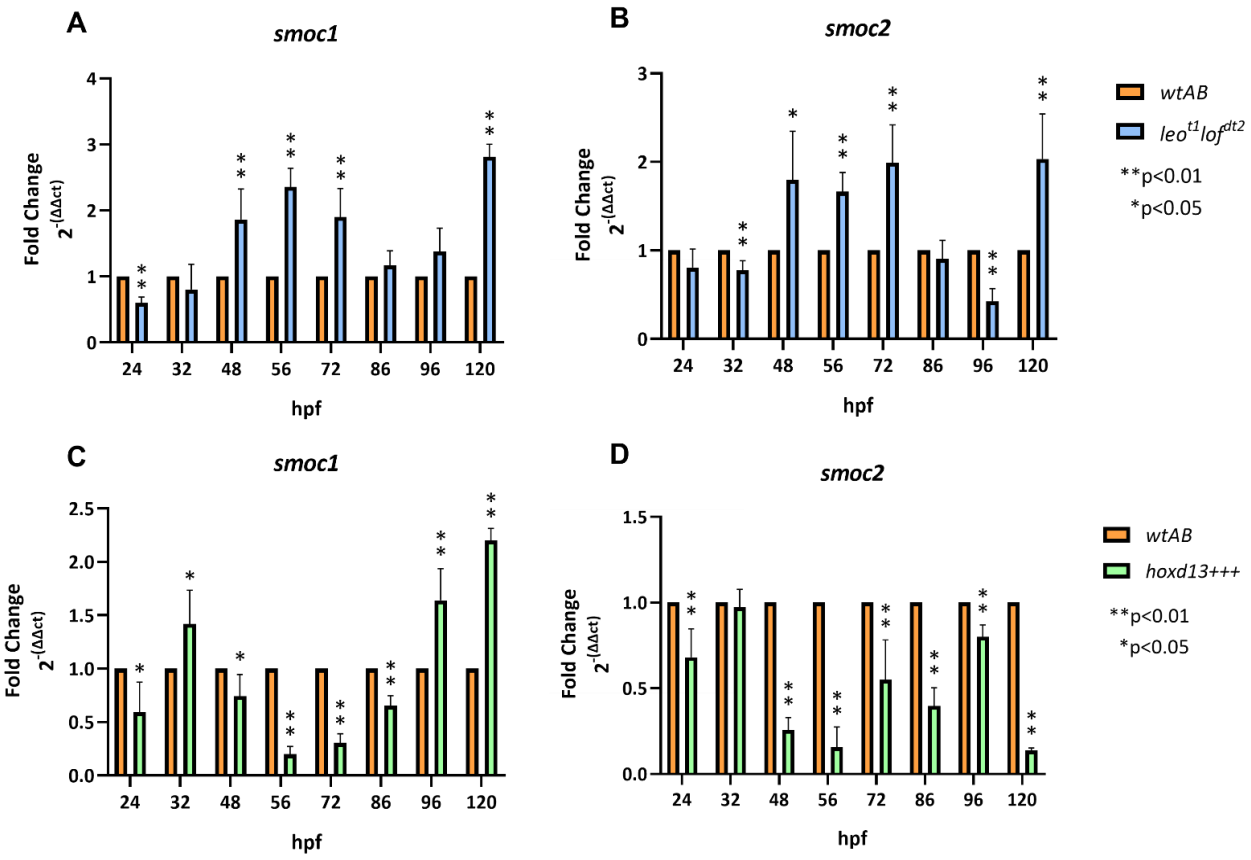

Figure 3.12: Comparison of *smoc1* and *smoc2* expression during fin development (RT-qPCR) in wild-type (*wtAB*), *leo*^{t1}*/lof*^{dt2} with longer finfolds, and *hsp70:hoxd13a* with shorter finfolds (*hoxd13+++*). Note that *leo*^{t1}*/lof*^{dt2} present general higher levels of expression of both genes. The line *hsp70:hoxd13a* has a peak at 32hpf for *smoc1*, shows lower expression levels at other stages after the heat shock and has higher levels at 96hpf and 120 hpf. Data analyzed with *t-test*, with p. value < 0.01 or <0.05.

3.4.2.2 *noggin3*

As for *noggin3*, we know that it represses BMP signaling by preventing the binding of BMP proteins to their receptors to activate the pathways intra-cellularly. In both the *wtAB* and *Leo*^{t1}*/Lof*^{dt2}, we found a curve of *noggin3* expression (Fig. 3.13) that reaches higher levels in the mutant condition since early stages (48hpf) and has a peak at 56hpf. In the *hoxd13a*-overexpressing condition, the most striking observation is the peak of expression at later stages.

When comparing the lines stage by stage (Fig. 3.14), we can see that the mutant condition also has higher levels of expression of *noggin3* (Fig. 3.14A). However, the most surprising result was the peak of expression at 32hpf in the transgenic line, right after the overexpression of *hoxd13a* (Fig. 3.14B). This is also, to our knowledge, the first indication that *Hoxd13* may regulate *noggin3* expression during fin/limb development, and that this can be an additional way to control the BMP signaling in the AER and finfold of Vertebrates.

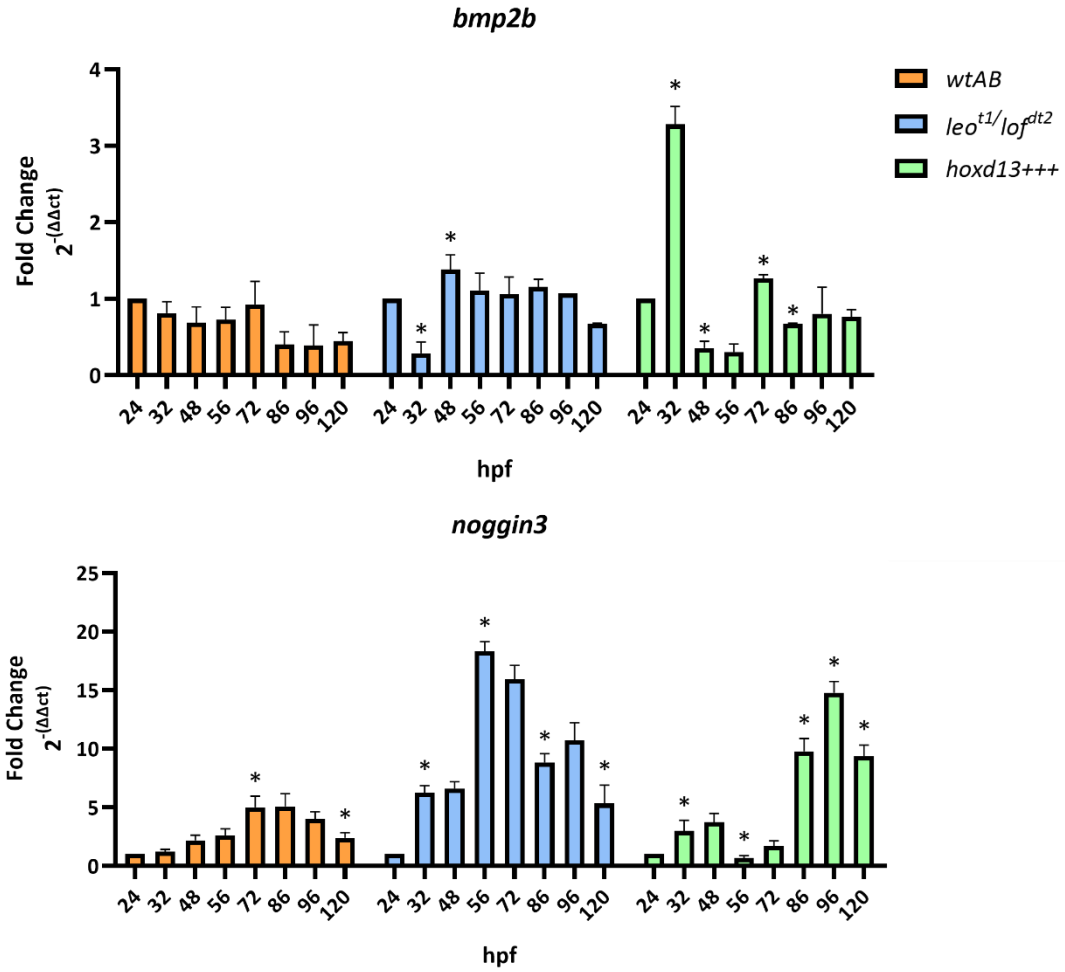

Figure 3.13: Expression dynamics of *noggin3* during fin development (RT-qPCR) in wild-type (*wtAB*), *leo*^{t1}*/lof*^{dt2} with longer finfolds, and *hsp70:hoxd13a* with shorter finfolds (*hoxd13*+++). Note the very high expression levels of the mutant condition. The transgenic line also presents higher expression in later stages. *´s represent the statistical significance between the designed stage and the previous one. These differences were calculated with a one-way ANOVA test, with p. value < 0.05.

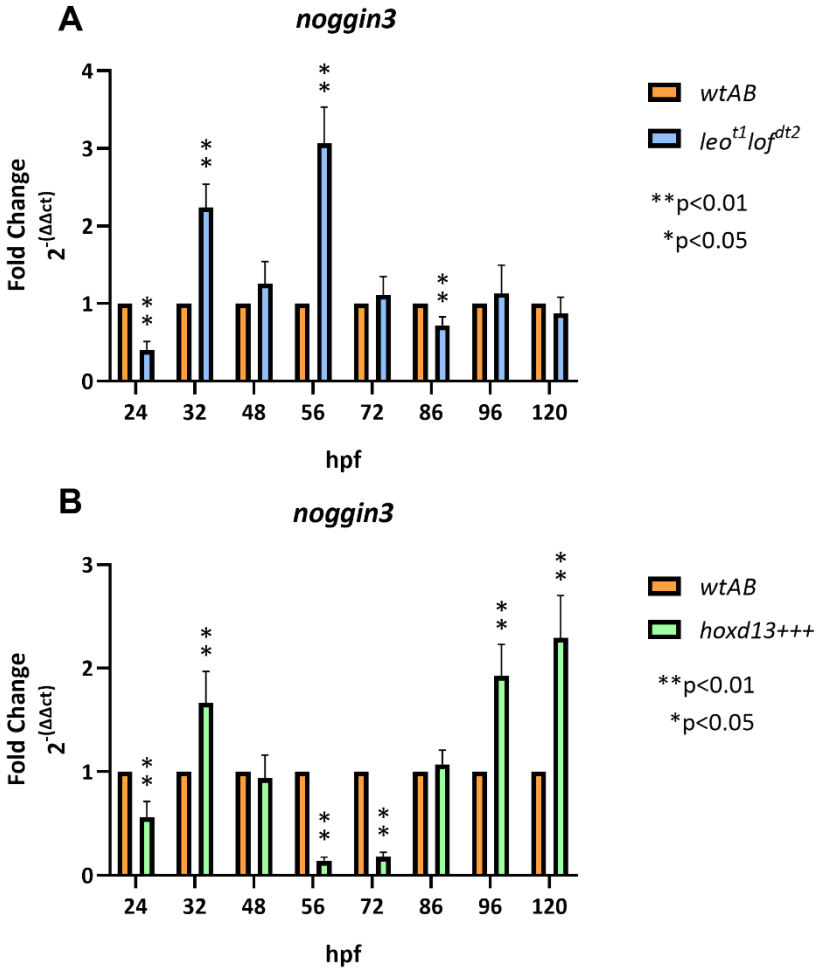

Figure 3.14: Comparison of *noggin3* expression during fin development (RT-qPCR) in wild-type (*wtAB*), *leo*^{t1}*/lof*^{dt2} with longer finfolds, and *hsp70:hoxd13a* with shorter finfolds (*hoxd13*+++). Note that *leo*^{t1}*/lof*^{dt2} present general higher levels of expression. The line *hsp70:hoxd13a* has a peak at 32hpf and at later stages. Data analyzed with *t-test*, with p. value <0.01 or <0.05.

3.4.2.3 *gremlin1a*

Regarding *grem1a,* it also represses BMP signaling (Ichinose et al., 2021). In both the *wtAB* and mutant line, we found a curve of expression that resembles the *noggin3* expression (Fig. 3.15). It also reaches higher levels of expression since early stages (32hpf) in the *Leo*^{t1}*/Lof*^{dt2} condition; at the same time that *bmp2b* has a moment of downregulation. As for the transgenic line, it seems to have an inverted profile of expression of *bmp2b*, especially at early and later stages.

As for the stage direct comparison, we found that *Leo^{t1}/Lof^{dt2}* has the same peak of expression at 32hpf and 72hpf (Fig. 3.16A). The *hoxd13a*-overexpressing condition shows higher expression at later stages, once again showing and inverted profile of *bmp2b* expression (Fig. 3.16B).

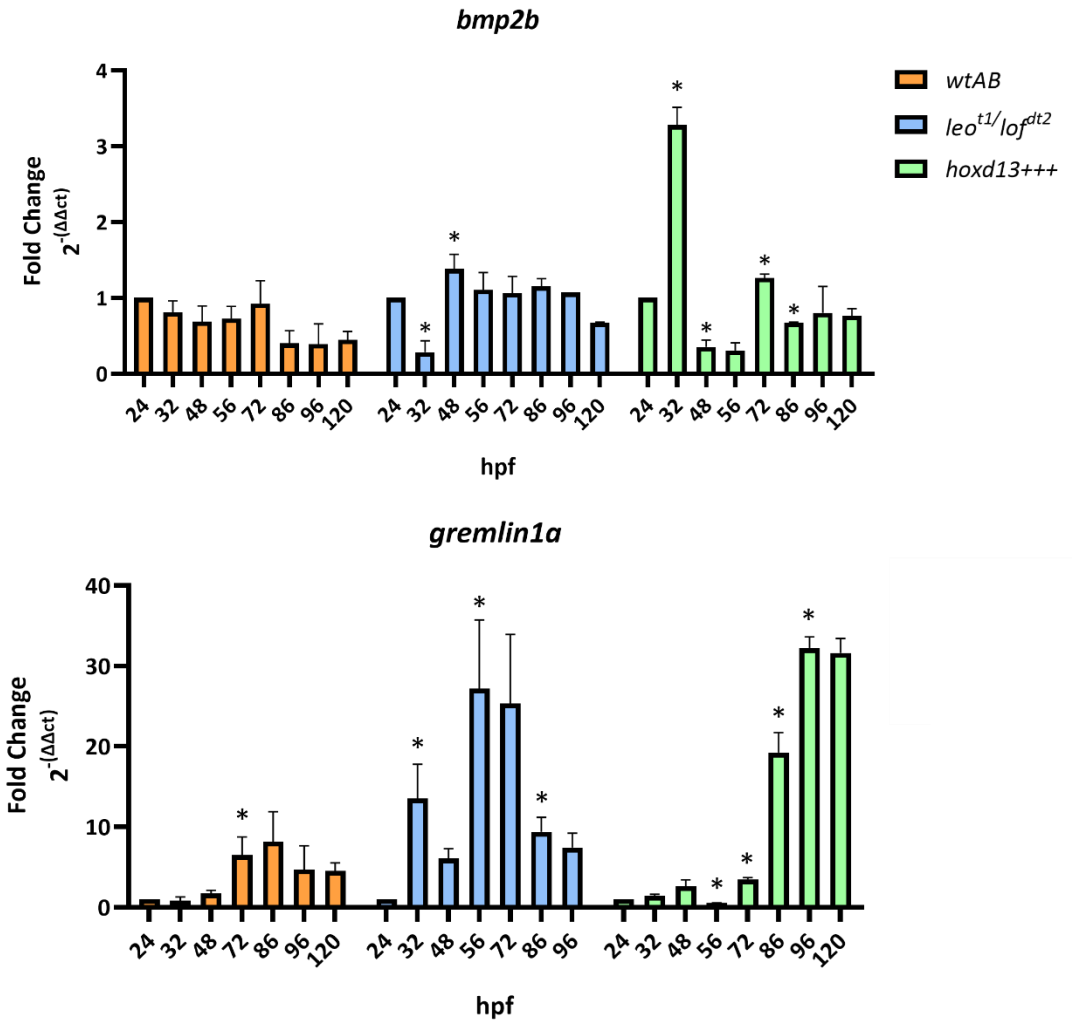

Figure 3.15: Expression dynamics of *gremlin1a* during fin development (RT-qPCR) in wild-type (*wtAB*), *leo^{t1}/lof^{dt2}* with longer finfolds, and *hsp70:hoxd13a* with shorter finfolds (*hoxd13*+++). Note the very high expression levels of the mutant condition and, at later stages, of the transgenic line. The *hoxd13*+++ condition shows an inverted profile of expression of the *bmp2b* levels. *´s represent the statistical significance between the designed stage and the previous one. These differences were calculated with a one-way ANOVA test, with p. value < 0.05.

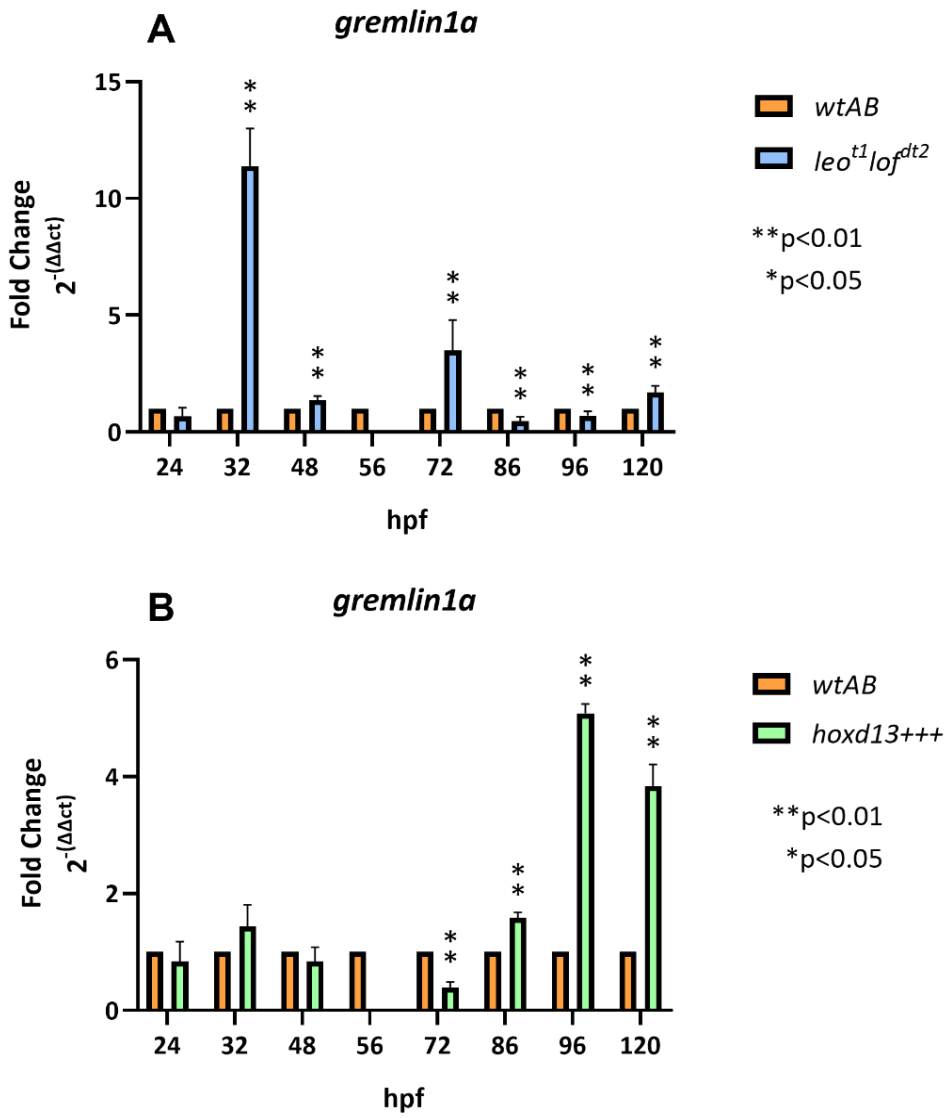

Figure 3.16: Comparison of *gremlin1a* expression during fin development (RT-qPCR) in wild-type (*wtAB*), *leo*^{t1}*/lof*^{dt2} with longer finfolds, and *hsp70:hoxd13a* with shorter finfolds (*hoxd13*+++). Note that *leo*^{t1}*/lof*^{dt2} present two peaks of expression, at 32hpf and 72hpf. The line *hsp70:hoxd13a* has a peak at later stages. Data analyzed with *t-test*, with p. value < 0.01 or <0.05. Data for the mutant and transgenic lines at 56hpf could not be obtained due to the lack of embryos.

3.5 Expression of downstream targets of the BMP signaling: *msx* genes

Muscle-segment homeobox genes (*msx*) are targets of the BMP signaling pathway, and they are important apoptosis effectors downstream of the *Shh/Gli3* pathway during limb development (Lallemand et al., 2009). We studied two *msx* genes known to be involved in the development of the pectoral fins in zebrafish: *msx1b* and *msx2b* (Akimenko et al., 1995).

Regarding *msx1b*, we detected expression in the mesenchyme under the finfold at 56hpf in both w*tAB* and *Leo*^{t1}*/Lof*^{dt2} fins (Fig. 3.17). However, the expression seems to be lower in the mutant condition. Taking in consideration the role of *msx* genes as apoptosis effectors, these data is consistent with the idea that mutant fins may have lower levels of apoptosis distally than the *wtAB* condition. Later, the expression becomes detectable throughout the finfold in *wtAB* fins while in *Leo*^{t1}*/Lof*^{dt2} mutants is maintained in the proximal part of the finfold. This may indicate that the shift of expression from the distal mesenchyme to the finfold is slower or delayed in the mutants. However, it is equally possible that the differential expression between the two conditions relates with areas with higher apoptosis rate at these states, which needs to be further investigated in the future with other methodological approaches. In the transgenic line, we identified a very similar expression pattern at 86hpf presented by the mutant condition at 120hpf. This may indicate that the transgenic line has, somehow, an accelerated development, which could be caused by the overexpression of *hoxd13a*, according to our hypothesis. Data for the transgenic line could not be obtained due to the high mortality rates associated with the heat shock treatment and the lack of embryos to perform equivalent experiments.

With respect to *msx2b*, we detected a different pattern of expression from *msx1b* (Fig. 3.18). In this case, *msx2b* was revealed to have a much stronger expression in mutant condition than in the *wtAB* at 56hpf. In addition, and contrarily to *msx1b*, the expression was throughout the finfold in L*eo*^{t1}*/Lof*^{dt2} fins and restricted to the distal part in the *wtAB* at this stage. Later, at 86hpf, the expression of *msx2b* is maintained in the finfold of the mutants, while it seems to be downregulated in the *wtAB* condition. These data suggest that *msx2b* may take longer to be downregulated in *Leo*^{t1}*/Lof*^{dt2} fins. In addition, the distinct expression pattern of *msx1b* and *msx2b* within the finfold and underlying mesenchyme suggests that *msx* genes may have different roles according to their domains of expression (Yoshida et al., 2020).

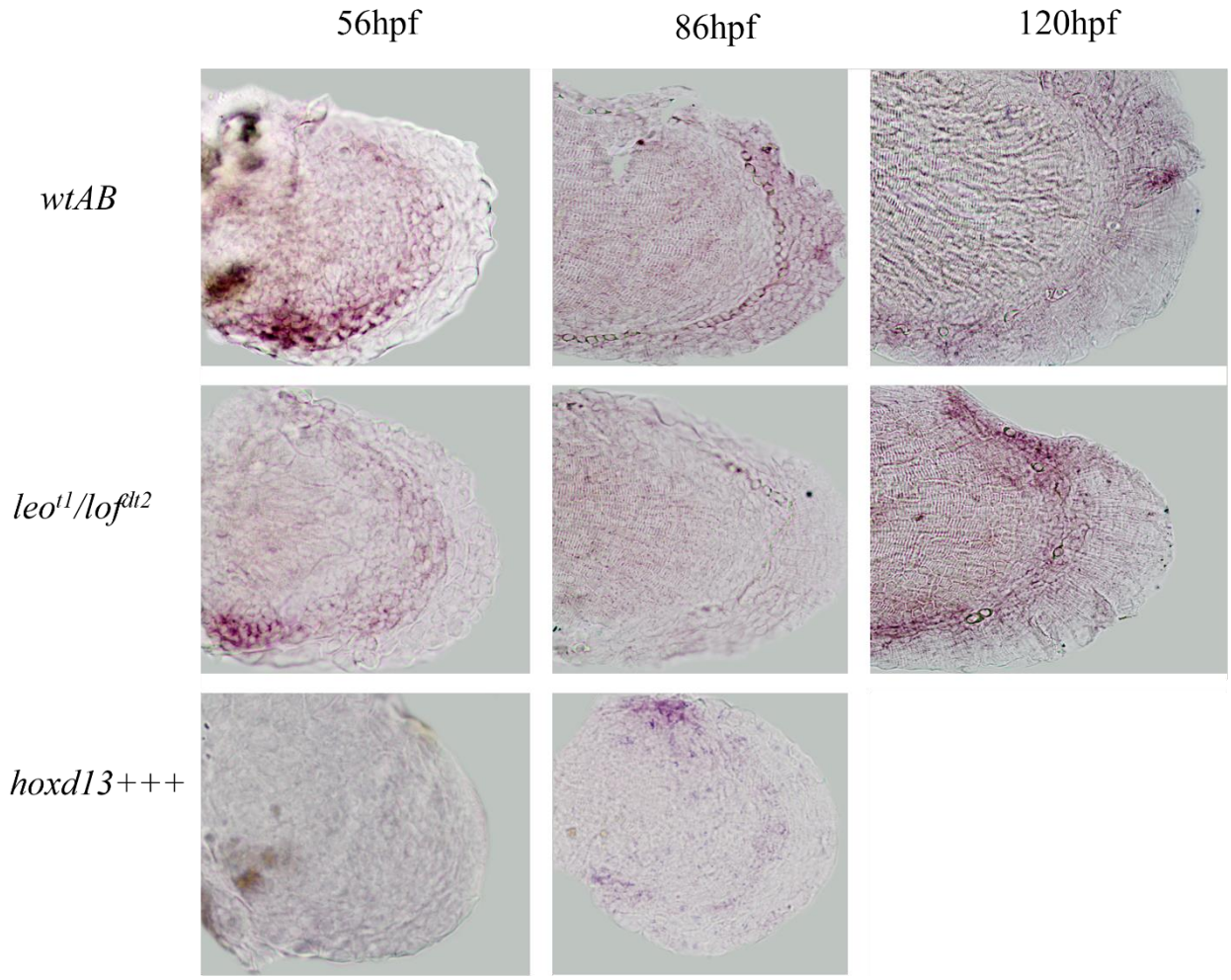

Figure 3.17 – Expression of *msx1b* detected by ISH in pectoral fins from wild-type *(wtAB)* *leo*^{t1}*/lof*^{dt2} mutants and *hoxd13+++* transgenics. Note the lower expression of *msx1b* in the mutant line at 56hpf, in comparison with the control, and distinct expression patterns at later stages: in the *wtAB*, it is throughout the finfold and, in the mutant, it is stronger in the proximal region of the finfold. The transgenic line shows no expression of this gene until 86hpf.

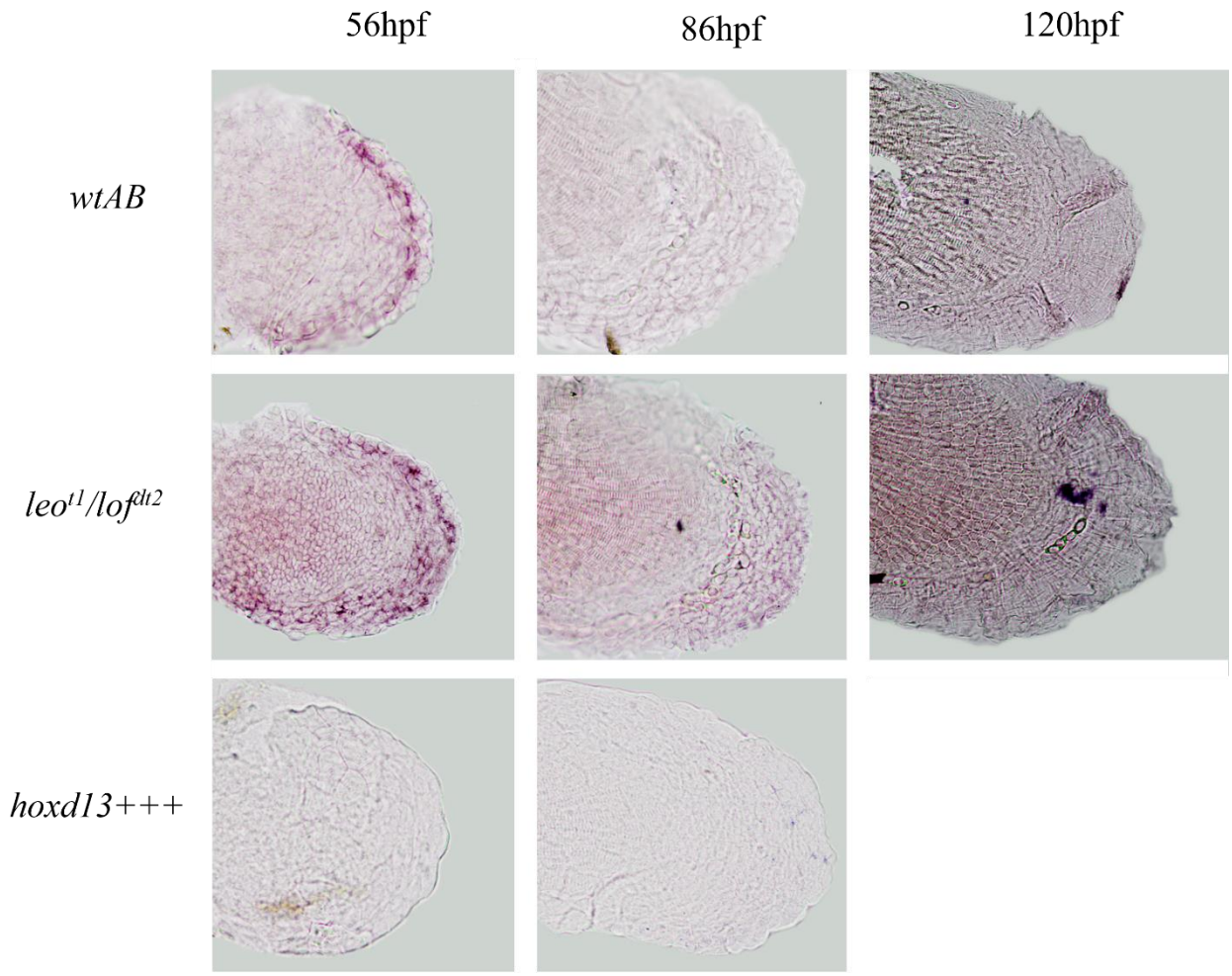

Figure 3.18 – Expression of *msx2b* detected by ISH in pectoral fins from wild-type *(wtAB)* *leo*^{t1}*/lof*^{dt2} mutants and *hoxd13+++* transgenics. Note the higher expression of *msx2b* in the mutant line at 56hpf, in comparison with the control, and distinct expression patterns at later stages: the downregulation at 86hpf specifically in the *wtAB* condition. The transgenic line shows no expression of this gene at the tested stages.

To gain further insight into the expression dynamics of *msx2b* in the different lines we performed RT-qPCR analyses throughout fin development (Fig. 3.19). We found that *msx2b* expression starts to decline after 32hpf in *wtAB* fins, while the same process is just detectable at 48hpf in *Leo*^{t1}*/Lof*^{dt2} fins. Regarding the *hoxd13a*-overexpressing line, we also found a peak of expression at 32hpf, immediately after the induction of the overexpression by heat shock. When we compared the expression between lines normalizing the expression to the wild-type condition

(Fig. 3.20), we detected that *msx2b* is significantly less transcribed in *Leo*^{t1}*/Lof*^{dt2} fins at 24hpf than in the controls and has a peak around 86hpf. Similar comparisons further confirm the upregulation of *msx2b* at 32hpf in the *hoxd13a*-overexpressing fins followed by a significant reduction in comparison with the wild-type condition, having also peaks at later stages. This is the first suggestion, to our knowledge that, *Hoxd13* expression may interfere with the expression of *msx* genes.

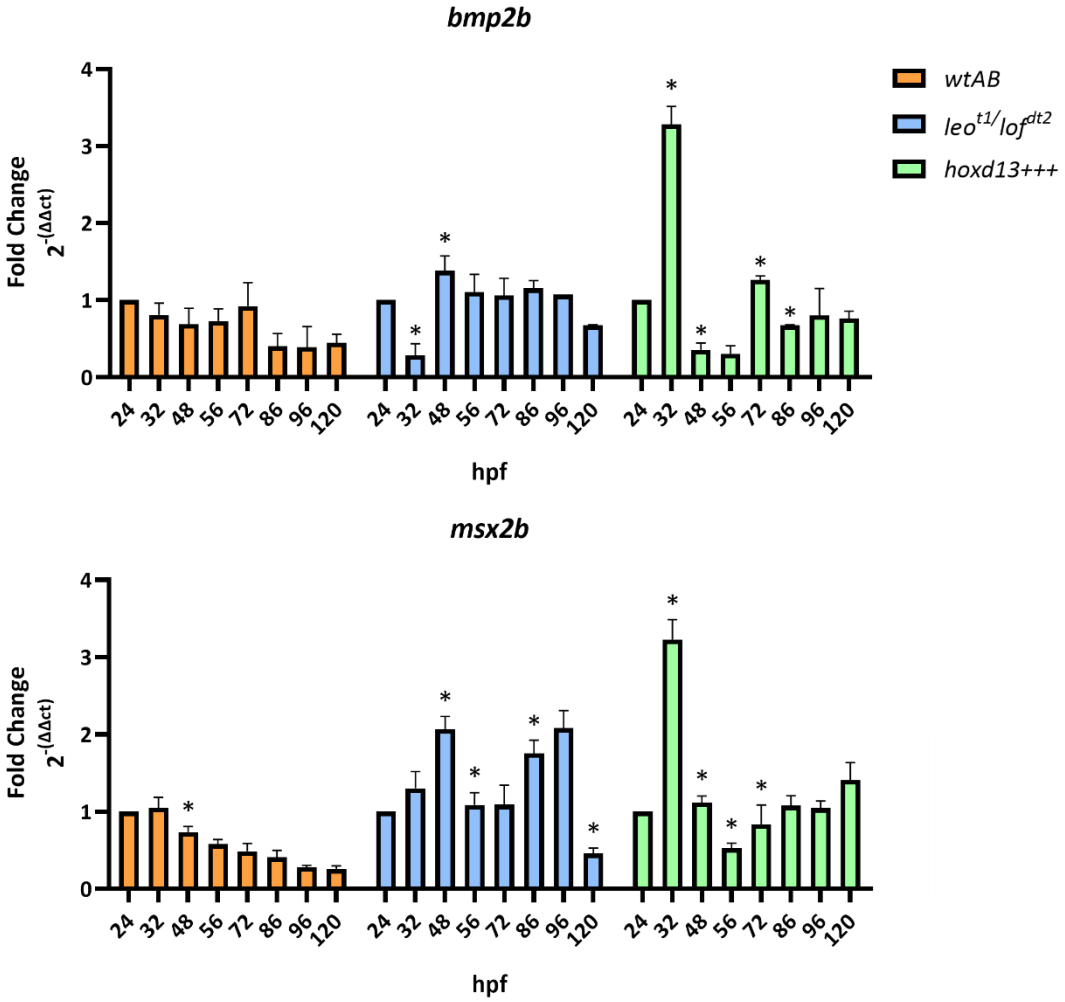

Figure 3.19 – Expression dynamics of *msx2b* during fin development (RT-qPCR) in wild-type *(wtAB)*, *leo*^{t1}*/lof*^{dt2} mutants, and *hoxd13a*-overexpressing fins (*hoxd13*+++). Note expression decline after 32hpf in *wtAB* and 48hpf in *leo*^{t1}*/lof*^{dt2} mutants, and the peak of expression at 32hpf in the *hoxd13*+++ condition, followed by a drastic decline, as in *bmp2b* levels.

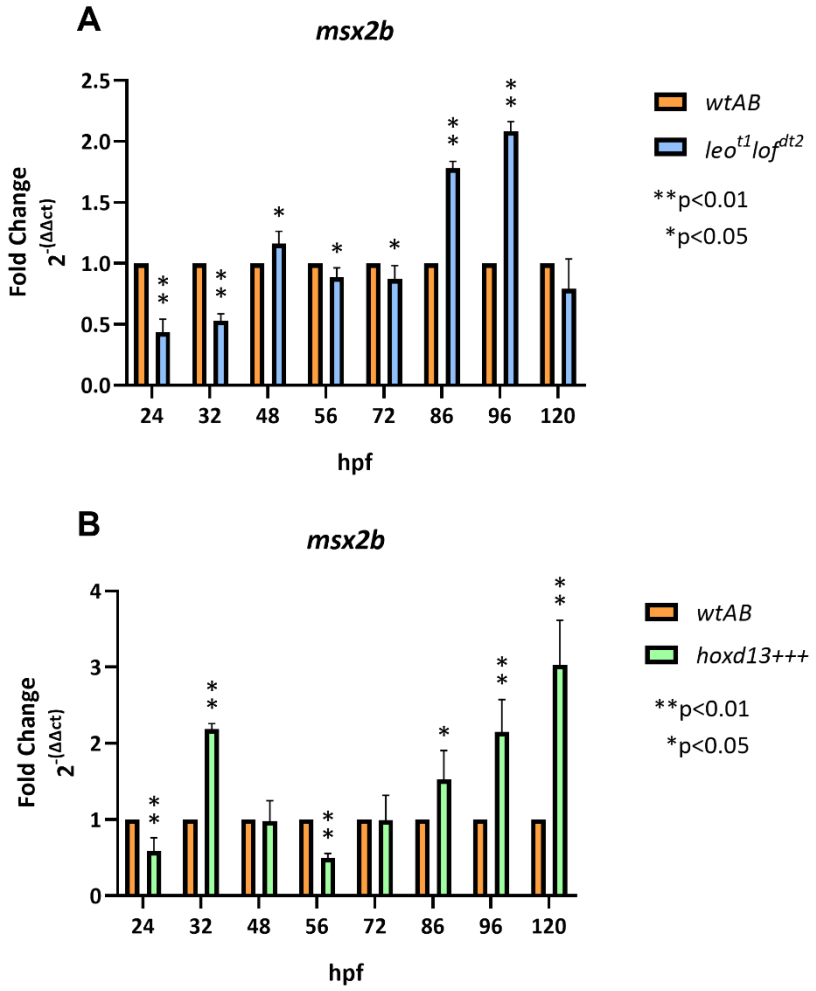

Figure 3.20 – Comparison of *msx2b* expression during fin development (RT-qPCR) in wild-type (*wtAB*), *leo*^{t1}*/lof*^{dt2} with longer finfolds, and *hsp70:hoxd13a* with shorter finfolds (*hoxd13*+++). Note that *leo*^{t1}*/lof*^{dt2} presents lower levels of expression at earlier stages but shifts to higher levels at later stages. The line *hsp70:hoxd13a* has a peak at 32hpf and at later stages. Data analyzed with *t-test*, with p. value < 0.01 or <0.05.

4. DISCUSSION

Modulation of *Hoxd13*, through the elaboration of its enhancer network, has been suggested as one of the mechanisms involved in the transition from fish fins to tetrapod limbs, namely by inducing the truncation of the finfold (Freitas et al., 2012). Recently, we proposed that *hoxd13a* modulation, the zebrafish orthologous, may lead to finfold reduction by interfering with the BMP signaling and potentiating localized apoptosis distally (Castro et al., 2021). Thus, this could have been a mechanism leading to the transition from fish fins to tetrapod limbs.

During the first part of this thesis, we contributed to this investigation by pursuing the analysis of fin development in a zebrafish mutant characterized by longer fins (Leo^{t1}/Lof^{dt2}). This zebrafish line has a mutation in a potassium channel responsible for the "longfin" phenotype, and that may shift normal cell electrical balance and trigger significant changes in genetic regulation (Cervera et al., 2016). In fact, the transcription rate factor is assumed to depend on the absolute value of the cell potential, which is dictated by the voltage-gated cell ion channels, and the interplay between genetic and electrical signals is thought to provide spatio-temporal information. Give that *Hoxd13* expression is influenced by the gradient of RA established in the limb bud (Francis et al., 1994; Wood et al., 1996), this differences in charges could lead to a longer time for RA to achieve the thresholds necessary to start influencing the expression of *hoxd13a* in zebrafish. As so, this gene would also need more time to start activating its targets, such as *bmp2b* and other BMP signaling-related genes, meaning that a simple temporal shift in the beginning of the process could delay the entire system, even though the rest of the network is working "just fine".

At first we 1) characterized the size of the finfold throughout development; 2) undertake expression analyses for a gene potentially involved in the BMP signaling and that was found to be modulated by *hoxd13a* in our previous assays, *bmp2b*; 3) explored if the *hoxd13a* and *bmp2b* expression levels related with the expression levels of genes involved in apoptosis (*casp3*) and proliferation (*ccnb1*), which was published in Castro et al (Castro et al., 2021). We then pursued a deeper characterization of the levels of expression of several components of the BMP signaling network in three zebrafish lines presenting distinct finfold sizes: the wild-type condition (*wtAB*), the long finfold Leo^{t1}/Lof^{dt2} condition, and the short finfold *hoxd13a*-overexpressing condition (*hoxd13*+++). Our main goal was to be able to correlate the expression of those genes with the size of the finfold in the distinct zebrafish lines. We found that all genes analyzed had distinct

expression profiles in each line and their expression was dynamic throughout fin development. Thus, our results straightened the hypothesis that BMP signaling modulation might have been the mechanism by which finfold size was reduced during evolution. In agreement with our ideas, *Bmp2* seems to limit the elongation of the AER in tetrapod models (Choi et al., 2012; Pizette & Niswander, 1999a) and inhibition of *Bmp2* function was also shown to increase the size of the AER (Maatouk et al., 2009).

In addition, *Bmp*'s expressed in the AER are important to control apoptosis, a key mechanism for digit patterning in tetrapods (Lin & Zhang, 2020), which has *msx* genes as effectors (Lallemand et al., 2009). We indeed found a connection between finfold size and the levels of *msx2b*, which suggest higher apoptosis in the finfold of *wtAB* and *hoxd13a*-overexpressing fins at certain stages than in the Leo^{t1}/Lof^{dt2} fins. Therefore, we suggest that, prior to the origin of tetrapods, and important role of the BMP signaling during fin development was to control apoptosis distally and define the finfold size. However, this mechanism might have been inherited by tetrapods and used to cause the apoptosis required for the patterning of the digits.

Another interesting data that came out from our studies is that the overexpression of *hoxd13a* seems to induce upregulation of several intervenient of the BMP signaling apart from *bmp2b*, such as *smad1*, *smoc1*, *noggin3* and *msx2b*. None of these genes have been reported as being direct downstream targets of *Hoxd13* (Salsi et al., 2008) and therefore we suggest that the impact of this transcription factor on the regulation of the BMP signaling-related genes might be indirect. However, Hoxd13 was reported to interact with some of the encoded proteins from these genes. For example, Hoxd13 and Smad1 were proposed to be co-factor in mice distal limb buds (Williams et al., 2005). In that study, the authors even suggest that: "HOX proteins may modulate Smad-mediated transcriptional activity through protein-protein interactions without the requirement for HOX monomeric DNA-binding capability". Taking this in consideration, we suggest that the role of Hoxd13 in the modulation of the finfold size during evolution could be also as a co-factor of Smad proteins that then activate apoptotic genes (*msx*), a hypothesis that should be further explored in the future.

As for the Leo^{t1}/Lof^{dt2} fins, apart from showing a reduction in *bmp2b* expression in comparison with the other lines, we encountered significant upregulation of *smoc1* and *smoc2*. Since they have been reported to be antagonists in several contexts, we suggest that an enhanced

smoc1 and *smoc2* expression might be the process responsible for reducing the levels of *bmp2b,* besides the influence that the lower levels of *hoxd13a* might also have in *bmp2b* regulation (Castro et al., 2021; Mateus et al., 2020). The antagonists *noggin3* and *gremlin1a* could also be involved in this process since its higher levels of expression are also correlated with lower levels of *bmp2b* expression in our study.

However, we propose that this may not be the only mechanism involved in the enlargement of the finfold in the mutant condition. Comparing the expression of all genes through fin development, we formulated an alternative hypothesis to "solve this puzzle"; despite *smad1,* all other BMP signaling-related genes were very low at 24hpf, and had a peak of expression at 48hpf. In the *wtAB* condition, an identical peak was detectable earlier, at 24hpf. These results suggest that the *hoxd13a/BMP* network is not downregulated in the mutants, but probably postponed in their development. This could also explain why the fins of this line seemed delayed in their development and with a morphology that suggests that they maintain undifferentiated cells in the finfold for longer.

Thus, our data suggests that finfold size, and the fin-to-limb transition in Vertebrates, may indeed relate with an heterochronic shift as proposed by Thorogood and Ferretti (Thorogood et al., 2010). They proposed that the shift was in the transition from an AER to a finfold and here we suggest the shift is related with an increment in *Hoxd13* expression distally that may trigger faster certain targets, such as several genes associated to the BMP signaling and, thus, activate processes that lead to finfold truncation, such as apoptosis or inhibition of actinotrichia formation, among others.

5. CONCLUSIONS

- This work contributed to explore how finfold size in zebrafish relates with the levels of *hoxd13a* and its targets involved in the BMP signaling pathway and to propose hypotheses regarding the molecular networks that may have allowed the fin-to-limb transition in Vertebrates.
- Our data helped to characterize the development of the long finfolds of the *Leo*^{t1}*/Lof*^{dt2} mutant and to determine that *hoxd13a* and its putative target *bmp2b* are less expressed in certain stages of this line in comparison with the *wtAB* controls. We also found that *msx* genes, the downstream apoptosis effectors of the BMP signaling pathway, are expressed differently according to the finfold size in three distinct zebrafish lines. For *msx2b*, we propose that its upregulation may trigger the apoptosis responsible for shorter finfolds in *hoxd13a*-overexpressing fins while its downregulation allows the formation of long finfolds in the *Leo*^{t1}*/Lof*^{dt2} mutant condition.
- Other elements of the BMP signaling seem to be upregulated in these mutants at certain stages; such is the case of *smoc1* and *smoc2*, known antagonists of the *Bmp* function. This leads us to propose that modulation of the finfold size through changes in the BMP signaling may have been also coordinated by upregulation of *smoc* genes distally during evolution.
- Analyses of gene expression using *hoxd13a*-overexpressing fins with shorter finfolds revealed that many elements of the BMP signaling are altered (*smad1*, *smoc1*, *noggin3*, and *msx2b*), which gives straight to the idea that *Hoxd13* modulation may have caused finfold truncation during evolution by interfering directly or indirectly with the BMP signaling in the finfold. Several observations suggest that finfold size may relate to "time". In the transgenic line (*hoxd13*+++), given that *hoxd13a* is overexpressed, it may trigger faster its targets, perhaps reducing the time required to reach important thresholds of expression and activate processes such as apoptosis or inhibition of actinotrichia formation, among others, that then lead to finfold truncation.
- In contrast, in the mutant line (*Leo*^{t1}*/Lof*^{dt2}), with lower expression of *hoxd13a*, its targets may take longer to reach the necessary thresholds and, therefore, the fin develops slower, with longer time in a proliferative state, allowing enough time to form long finfolds, before processes such as apoptosis start to cause inhibition of their growth.

- In light of our data, we embrace the idea that the fin-to-limb transition is due to a heterochronic shift, but we propose a novel molecular mechanism involved in it: acceleration of the BMP signaling in the finfold promoted by higher levels of *Hoxd13*. Maybe the time "saved" with accelerated differentiation could have left "free time" for the development of new mechanisms that then potentiated the formation of novel structures, progressively more complex, until evolution reached the autopod of tetrapods.

Bibliography

Abbasi, A.A (2008). *GLI genes: Cis- Acting Regulatory Elements. Dissertation* https://archiv.ub.uni-marburg.de/diss/z2008/0410/pdf/daaa.pdf

Abe, G., & Ota, K. G. (2017). Evolutionary developmental transition from median to paired morphology of Vertebrate fins: Perspectives from twin-tail goldfish. *Developmental Biology*, *427*(2), 251–257. https://doi.org/10.1016/j.ydbio.2016.11.022

Ahn, D., & Ho, R. K. (2008). Tri-phasic expression of posterior Hox genes during development of pectoral fins in zebrafish: Implications for the evolution of Vertebrate paired appendages. *Developmental Biology*, *322*(1), 220–233. https://doi.org/10.1016/j.ydbio.2008.06.032

Akimenko, M. A., Johnson, S. L., Westerfield, M., & Ekker, M. (1995). Differential induction of four msx homeobox genes during fin development and regeneration in zebrafish. *Development*, *121*(2), 347–357. https://doi.org/10.1242/dev.121.2.347

Amores, A., Force, A., Yan, Y. L., Joly, L., Amemiya, C., Fritz, A., Ho, R. K., Langeland, J., Prince, V., Wang, Y. L., Westerfield, M., Ekker, M., & Postlethwait, J. H. (1998). Zebrafish hox clusters and Vertebrate genome evolution. *Science*, *282*(5394), 1711–1714. https://doi.org/10.1126/science.282.5394.1711

Andrade-Rocha, F. (2017). On the origins of the semen analysis: A close relationship with the history of the reproductive medicine. In *Journal of Human Reproductive Sciences*. https://doi.org/10.4103/jhrs.JHRS_97_17

Beccari, L., Jaquier, G., Lopez-Delisle, L., Rodriguez-Carballo, E., Mascrez, B., Gitto, S., Woltering, J., & Duboule, D. (2021). Dbx2 regulation in limbs suggests interTAD sharing of enhancers. *Developmental Dynamics*, *November 2020*, 1–20. https://doi.org/10.1002/dvdy.303

Bruce, A. E. E., Oates, A. C., Prince, V. E., & Ho, R. K. (2001). Additional hox clusters in the zebrafish: Divergent expression patterns belie equivalent activities of duplicate hoxB5 genes. *Evolution and Development*, *3*(3), 127–144. https://doi.org/10.1046/j.1525-142X.2001.003003127.x

Castro, J., Beviano, V., Paço, A., Leitão-Castro, J., Cadete, F., Francisco, M., & Freitas, R. (2021). Hoxd13/Bmp2-mediated mechanism involved in zebrafish finfold design. *Scientific Reports*, *11*(1), 7165. https://doi.org/10.1038/s41598-021-86621-4

Cervera, J., Meseguer, S., & Mafe, S. (2016). The interplay between genetic and bioelectrical signaling permits a spatial regionalisation of membrane potentials in model multicellular ensembles. *Scientific Reports*, *6*(September), 1–15. https://doi.org/10.1038/srep35201

Choi, K. S., Lee, C., Maatouk, D. M., & Harfe, B. D. (2012). Bmp2, Bmp4 and Bmp7 are co-required in the mouse AER for normal digit patterning but not limb outgrowth. *PLoS ONE*, *7*(5), 1–8. https://doi.org/10.1371/journal.pone.0037826

Das De, S., & Sebastin, S. J. (2019). Considerations in Flap Selection for Soft Tissue Defects of the Hand. *Clinics in Plastic Surgery*, *46*(3), 393–406. https://doi.org/10.1016/j.cps.2019.03.010

de Bessa Garcia, S. A., Araújo, M., Pereira, T., Mouta, J., & Freitas, R. (2020). HOX genes function in Breast Cancer development. *Biochimica et Biophysica Acta - Reviews on Cancer*, *1873*(2), 188358. https://doi.org/10.1016/j.bbcan.2020.188358

De Caestecker, M. (2004). The transforming growth factor-β superfamily of receptors. *Cytokine and Growth Factor Reviews*, *15*(1), 1–11. https://doi.org/10.1016/j.cytogfr.2003.10.004

Diogo, R. (2020). Cranial or postcranial—Dual origin of the pectoral appendage of Vertebrates combining the fin-fold and gill-arch theories? *Developmental Dynamics*, *249*(10), 1182–1200. https://doi.org/10.1002/dvdy.192

Dooley, K., & Zon, L. I. (2000). Zebrafish: A model system for the study of human disease. *Current Opinion in Genetics and Development*, *10*(3), 252–256. https://doi.org/10.1016/S0959-437X(00)00074-5

Edwards, K., Logan, J., & Saunders, N. (2005). Real-Time PCR : An Essential Guide Textbook – Atlas of Intestinal Infection in AIDS Public Health Response to Biological and Chemical Weapons : WHO Guidance. *Emerging Infectious Diseases*, *11*(1), 1–2.

Francis, P. H., Richardson, M. K., Brickell, P. M., & Tickle, C. (1994). Bone morphogenetic proteins and a signalling pathway that controls patterning in the developing chick limb. *Development*, *120*(1), 209–218. https://doi.org/10.1242/dev.120.1.209

Freitas, R., Gómez-Marín, C., Wilson, J. M., Casares, F., & Gómez-Skarmeta, J. L. (2012). Hoxd13 Contribution to the Evolution of Vertebrate Appendages. *Developmental Cell*, *23*(6), 1219–1229. https://doi.org/10.1016/j.devcel.2012.10.015

Freitas, R., Gómez-Skarmeta, J. L., & Rodrigues, P. N. (2014). New frontiers in the evolution of fin development. *Journal of Experimental Zoology Part B: Molecular and Developmental Evolution*, *322*(7), 540–552. https://doi.org/10.1002/jez.b.22563

Freitas, R., Zhang, G. J., & Cohn, M. J. (2006). Evidence that mechanisms of fin development evolved in the midline of early Vertebrates. *Nature*, *442*(7106), 1033–1037. https://doi.org/10.1038/nature04984

Freitas, R., Zhang, G. J., & Cohn, M. J. (2007). Biphasic Hoxd gene expression in shark paired fins reveals an ancient origin of the distal limb domain. *PLoS ONE*, *2*(8). https://doi.org/10.1371/journal.pone.0000754

Garcia, S. A. de B., Araújo, M., & Freitas, R. (2020). Dataset of HOXB7, HOXB8 and HOXB9 expression profiles in cell lines representative of the breast cancer molecular subtypes Luminal a (MCF7), Luminal b (BT474), HER2+ (SKBR3) and triple-negative (MDA231, MDA468), compared to a model of normal cells (MCF10A. *Data in Brief*, *30*, 3–8. https://doi.org/10.1016/j.dib.2020.105572

Grandel, H., & Schulte-Merker, S. (1998). The development of the paired fins in the zebrafish (Danio rerio). *Mechanisms of Development*, *79*(1–2), 99–120. https://doi.org/10.1016/S0925-4773(98)00176-2

Haro, E., Delgado, I., Junco, M., Yamada, Y., Mansouri, A., Oberg, K. C., & Ros, M. A. (2014). Sp6 and Sp8 Transcription Factors Control AER Formation and Dorsal-Ventral Patterning in Limb Development. *PLoS Genetics*, *10*(8). https://doi.org/10.1371/journal.pgen.1004468

Harris, B. Y. J. E. (1936). The Role of the Fins in the Equilibrium of the Swimming Fish: I. Wind-Tunnel Tests on a Model of Mustelus canis (Mitchill). *Journal of Experimental Biology*, *13*(4), 476–493.

Hollnagel, A., Oehlmann, V., Heymer, J., Rüther, U., & Nordheim, A. (1999). Id genes are direct targets of bone morphogenetic protein induction in embryonic stem cells. *Journal of Biological Chemistry*, *274*(28), 19838–19845. https://doi.org/10.1074/jbc.274.28.19838

Ichinose, M., Suzuki, N., Wang, T., Kobayashi, H., Vrbanac, L., Ng, J. Q., Wright, J. A., Lannagan, T. R. M., Gieniec, K. A., Lewis, M., Ando, R., Enomoto, A., Koblar, S., Thomas, P., Worthley, D. L., & Woods, S. L. (2021). The BMP antagonist gremlin 1 contributes to the development of cortical excitatory neurons, motor balance and fear responses. *Development*, *148*(14). https://doi.org/10.1242/dev.195883

Janvier, P. (1996). Early Vertebrates. Oxford Monographs on Geology and Geophysics, Volume 33. xiii + Oxford: Clarendon Press.

Kimmel, C. B., Ballard, W. W., Kimmel, S. R., Ullmann, B., & Schilling, T. F. (1995). Stages of embryonic development of the zebrafish. *Developmental Dynamics*, *203*(3), 253–310. https://doi.org/10.1002/aja.1002030302

Kubista, M., Andrade, J. M., Bengtsson, M., Forootan, A., Jonák, J., Lind, K., Sindelka, R., Sjöback, R., Sjögreen, B., Strömbom, L., Ståhlberg, A., & Zoric, N. (2006). The real-time polymerase chain reaction. *Molecular Aspects of Medicine*, *27*(2–3), 95–125. https://doi.org/10.1016/j.mam.2005.12.007

Kuraku, S. (2011). Hox gene clusters of early Vertebrates: Do they serve as reliable markers for genome evolution? *Genomics, Proteomics and Bioinformatics*, *9*(3), 97–103. https://doi.org/10.1016/S1672-0229(11)60012-0

Kurosaka, H., Wang, Q., Sandell, L., Yamashiro, T., & Trainor, P. A. (2017). Rdh10 loss-of-function and perturbed retinoid signaling underlies the etiology of choanal atresia. *Human Molecular Genetics*, *26*(7), 1268–1279. https://doi.org/10.1093/hmg/ddx031

Lacalli, T. (2012). The Middle Cambrian fossil Pikaia and the evolution of chordate swimming. *EvoDevo*, *3*(1), 1. https://doi.org/10.1186/2041-9139-3-12

Lallemand, Y., Bensoussan, V., Cloment, C. Saint, & Robert, B. (2009). Msx genes are important apoptosis effectors downstream of the Shh/Gli3 pathway in the limb. *Developmental Biology*, *331*(2), 189–198. https://doi.org/10.1016/j.ydbio.2009.04.038

Lalonde, R. L., Moses, D., Zhang, J., Cornell, N., Ekker, M., & Akimenko, M. A. (2016). Differential actinodin1 regulation in zebrafish and mouse appendages. *Developmental Biology*, *417*(1), 91–103. https://doi.org/10.1016/j.ydbio.2016.05.019

Lappin, T. R. J., Grier, D. G., Thompson, A., & Halliday, H. L. (2006). HOX genes: Seductive science, mysterious mechanisms. *Ulster Medical Journal*, *75*(1), 23–31.

Lettice, L. A., Heaney, S. J. H., Purdie, L. A., Li, L., de Beer, P., Oostra, B. A., Goode, D., Elgar, G., Hill, R. E., & de Graaff, E. (2003). A long-range Shh enhancer regulates expression in the developing limb and fin and is associated with preaxial polydactyly. *Human Molecular Genetics*, *12*(14), 1725–1735. https://doi.org/10.1093/hmg/ddg180

Lin, G. hao, & Zhang, L. (2020). Apical ectodermal ridge regulates three principal axes of the developing limb. *Journal of Zhejiang University: Science B*, *21*(10), 757–766. https://doi.org/10.1631/jzus.B2000285

Loucks, E., & Ahlgren, S. (2012). Assessing teratogenic changes in a zebrafish model of fetal alcohol exposure. *Journal of Visualized Experiments : JoVE*, *61*, 1–7. https://doi.org/10.3791/3704

Luo, Z., Rhie, S. K., & Farnham, P. J. (2019). The enigmatic hox genes: Can we crack their code? *Cancers*, *11*(3). https://doi.org/10.3390/cancers11030323

Maatouk, D. M., Choi, K. S., Bouldin, C. M., & Harfe, B. D. (2009). In the limb AER Bmp2 and Bmp4 are required for dorsal-ventral patterning and interdigital cell death but not limb outgrowth. *Developmental Biology*, *327*(2), 516–523. https://doi.org/10.1016/j.ydbio.2009.01.004

Mateus, R., Holtzer, L., Seum, C., Hadjivasiliou, Z., Dubois, M., Jülicher, F., & Gonzalez-Gaitan, M. (2020). BMP Signaling Gradient Scaling in the Zebrafish Pectoral Fin. *Cell Reports*, *30*(12), 4292-4302.e7. https://doi.org/10.1016/j.celrep.2020.03.024

Nagashima, H., Sugahara, F., Watanabe, K., Shibata, M., Chiba, A., & Sato, N. (2016). Developmental origin of the clavicle, and its implications for the evolution of the neck and the paired appendages in Vertebrates. *Journal of Anatomy*, *229*(4), 536–548. https://doi.org/10.1111/joa.12502

Needham, Joseph. *A History of Embryology*. New York: Abelard-Schuman, 1959

Paço, A., & Freitas, R. (2018). Hox D genes and the fin-to-limb transition: Insights from fish studies. *Genesis*, *56*(1), 1–9. https://doi.org/10.1002/dvg.23069

Peluso, S., Douglas, A., Hill, A., de Angelis, C., Moore, B. L., Grimes, G., Petrovich, G., Essafi, A., & Hill, R. E. (2017). Fibroblast growth factors (FGFs) prime the limb specific shh enhancer for chromatin changes that balance histone acetylation mediated by e26 transformation-specific (ETS) factors. *ELife*, *6*, 1–22. https://doi.org/10.7554/eLife.28590

Pieretti, J., Gehrke, A. R., Schneider, I., Adachi, N., Nakamura, T., & Shubin, N. H. (2015). Organogenesis in deep time: A problem in genomics, development, and paleontology. *Proceedings of the National Academy of Sciences of the United States of America*, *112*(16), 4871–4876. https://doi.org/10.1073/pnas.1403665112

Pignatti, E., Zeller, R., & Zuniga, A. (2014). To BMP or not to BMP during Vertebrate limb bud development. *Seminars in Cell and Developmental Biology*, *32*, 119–127. https://doi.org/10.1016/j.semcdb.2014.04.004

Pizette, S., & Niswander, L. (1999a). BMPs negatively regulate structure and function of the limb apical ectodermal ridge. *Development*, *126*(5), 883–894. https://doi.org/10.1242/dev.126.5.883

Pizette, S., & Niswander, L. (1999b). *Development 1999 Pizette*. *894*, 1–12. papers://34147092-be8b-4114-bd76-f22a3f34067a/Paper/p61

Riley, C., Cloutier, R., & Grogan, E. D. (2017). Similarity of morphological composition and

developmental patterning in paired fins of the elephant shark. *Scientific Reports*, *7*(1), 1–10. https://doi.org/10.1038/s41598-017-10538-0

Royle, S. R., Tabin, C. J., & Young, J. J. (2021). Limb positioning and initiation: an evolutionary context of pattern and formation. *Developmental Dynamics*, *January*, 1–16. https://doi.org/10.1002/dvdy.308

Salsi, V., Vigano, M. A., Cocchiarella, F., Mantovani, R., & Zappavigna, V. (2008). Hoxd13 binds in vivo and regulates the expression of genes acting in key pathways for early limb and skeletal patterning. *Developmental Biology*, *317*(2), 497–507. https://doi.org/10.1016/j.ydbio.2008.02.048

Sánchez-Herrero, E. (2013). Hox Targets and Cellular Functions. *Scientifica*, *2013*, 1–26. https://doi.org/10.1155/2013/738257

Shubin, N. H., Daeschler, E. B., & Jenkins, F. A. (2006). The pectoral fin of Tiktaalik roseae and the origin of the tetrapod limb. *Nature*, *440*(7085), 764–771. https://doi.org/10.1038/nature04637

Shubin, N., Tabin, C., & Carroll, S. (1997). Fossils, genes and the evolution of animal limbs. *Nature*, *388*(6643), 639–648. https://doi.org/10.1038/41710

Stepanow, S., Honolka, J., Gambardella, P., Vitali, L., Abdurakhmanova, N., Tseng, T. C., Rauschenbach, S., Tait, S. L., Sessi, V., Klyatskaya, S., Ruben, M., Kern, K., Atanasov, M., Aravena, D., Suturina, E., Bill, E., Maganas, D., Neese, F., Atzori, M., … Bu, X. H. (2010). {\copyright} 19 9 3 Nature Publishing Group. *Journal of the American Chemical Society*, *132*(29), 2517–2528. https://doi.org/10.1016/j.ccr.2020.213617%0Ahttp://dx.doi.org/10.1016/j.ccr.2014.11.016

Stephens, T. D., Baker, W. C., Cotterell, J. W., Edwards, D. R., Pugmire, D. S., Roberts, S. G., Shaker, M. R., Willis, H. J., & Winger, K. P. (1993). Evaluation of the chick wing territory as an equipotential self-differentiating system. *Developmental Dynamics*, *197*(3), 157–168. https://doi.org/10.1002/aja.1001970302

Tamura, K., Yonei-Tamura, S., Yano, T., Yokoyama, H., & Ide, H. (2008). The autopod: Its formation during limb development. *Development Growth and Differentiation*, *50*(SUPPL. 1). https://doi.org/10.1111/j.1440-169X.2008.01020.x

Tarazona, O. A., Lopez, D. H., Slota, L. A., & Cohn, M. J. (2019). Evolution of limb development in cephalopod mollusks. *ELife*, *8*, 1–19. https://doi.org/10.7554/eLife.43828.001

Te Welscher, P., Zuniga, A., Kuijper, S., Drenth, T., Goedemans, H. J., Meijlink, F., & Zeller, R. (2002). Progression of Vertebrate limb development through SHH-mediated counteraction of GLI3. *Science*, *298*(5594), 827–830. https://doi.org/10.1126/science.1075620

Thisse, C., & Thisse, B. (2008). High-resolution in situ hybridization to whole-mount zebrafish embryos. *Nature Protocols*, *3*(1), 59–69. https://doi.org/10.1038/nprot.2007.514

Tickle, C. (2015). How the embryo makes a limb: Determination, polarity and identity. *Journal of Anatomy*, *227*(4), 418–430. https://doi.org/10.1111/joa.12361

Tickle, C., & Towers, M. (2017). Sonic hedgehog signaling in limb development. *Frontiers in Cell and Developmental Biology*, *5*(FEB), 1–19. https://doi.org/10.3389/fcell.2017.00014

Towers, M. (2018). Evolution of antero-posterior patterning of the limb: Insights from the chick. *Genesis*, *56*(1), 1–15. https://doi.org/10.1002/dvg.23047

Wang, R. N., Green, J., Wang, Z., Deng, Y., Qiao, M., Peabody, M., Zhang, Q., Ye, J., Yan, Z., Denduluri, S., Idowu, O., Li, M., Shen, C., Hu, A., Haydon, R. C., Kang, R., Mok, J., Lee, M. J., Luu, H. L., & Shi, L. L. (2014). Bone Morphogenetic Protein (BMP) signaling in development and human diseases. *Genes and Diseases*, *1*(1), 87–105. https://doi.org/10.1016/j.gendis.2014.07.005

Wellik, D. M., Hawkes, P. J., & Capecchi, M. R. (2002). Hox11 paralogous genes are essential for metanephric kidney induction. *Genes and Development*, *16*(11), 1423–1432. https://doi.org/10.1101/gad.993302

Williams, T. M., Williams, M. E., Heaton, J. H., Gelehrter, T. D., & Innis, J. W. (2005). Group 13 HOX proteins interact with the MH2 domain of R-Smads and modulate Smad transcriptional activation functions independent of HOX DNA-binding capability. *Nucleic Acids Research*, *33*(14), 4475–4484. https://doi.org/10.1093/nar/gki761

Woltering, J. M., Irisarri, I., Ericsson, R., Joss, J. M. P., Sordino, P., & Meyer, A. (2020). Sarcopterygian fin ontogeny elucidates the origin of hands with digits. *Science Advances*, *6*(34), 1–7. https://doi.org/10.1126/sciadv.abc3510

Wood, H. B., Ward, S. J., & Morriss-Kay, G. M. (1996). Effects of all-trans-retinoic acid on skeletal pattern, 5'HoxD gene expression, and RARβ2/β4 promoter activity in embryonic mouse limbs. *Developmental Genetics*, *19*(1), 74–84. https://doi.org/10.1002/(SICI)1520-6408(1996)19:1<74::AID-DVG8>3.0.CO;2-Y

Yoshida, K., Kawakami, K., Abe, G., & Tamura, K. (2020). Zebrafish can regenerate endoskeleton in larval pectoral fin but the regenerative ability declines. *Developmental Biology*, *463*(2), 110–123. https://doi.org/10.1016/j.ydbio.2020.04.010

Zhang, J., Wagh, P., Guay, D., Sanchez-Pulido, L., Padhi, B. K., Korzh, V., Andrade-Navarro, M. A., & Akimenko, M. A. (2010). Loss of fish actinotrichia proteins and the fin-to-limb transition. *Nature*, *466*(7303), 234–237. https://doi.org/10.1038/nature09137

Zuniga, A. (2015). Next generation limb development and evolution: Old questions, new perspectives. *Development (Cambridge)*, *142*(22), 3810–3820. https://doi.org/10.1242/dev.125757